Imperial College of Science and Technology

DEPARTMENT OF AERONAUTICS

London SW7 2BY

I.C. Aero Report 81-02 1981

RAREFIED HYPERSONIC FLOW ABOUT A FLAT-ENDED CIRCULAR CYLINDER

by

R.G. Dominy, M.N. Macrossan, J.K. Harvey

SUMMARY

The rarefied Mach 25 flow about a flat-ended cylinder is calculated using the Monte-Carlo direct simulation technique. Collisions between diatomic molecules are calculated using three collision models incorporating approximate classical or phenomenological models of internal-external energy exchange.

Simulation results for each collision model are found to be in good agreement with electron beam density surveys in the stagnating flow ahead of the cylinder. Heat transfer is found to be sensitive to the collision model used but within the scatter of published data. It is suggested that measurements of temperature profiles in the stagnation region would allow better evaluation of the collision models.

ISSN 0308-7247

This work was supported by the Ministry of Defence under Research Agreement Number AT-2037-084

NOMENCLATURE

a = potential parameter = $4.02 \times 10^{10} m^{-1}$ (Pullin, 1974)

b = collision impact parameter (initial trajectory separation)

$\bar{c}$ = mean thermal speed = $(8kT/\pi m)^{\frac{1}{2}}$

$\bar{c}_w$ = mean speed of molecules emitted from surface $(9\pi kT_w/8m)^{\frac{1}{2}}$

C_h = Stanton number $\equiv q/(\rho_\infty U_\infty (H_0 - H_w))$

C^* = $\mu^* T_\infty / \mu_\infty T^*$

d = hard sphere molecule radius for N_2
= 3.78Å (Bird, 1976, App. A)

e_{cm} = total centre of mass energy of collision

g = relative velocity of collision

H = enthalpy

$I, \hat{I}$ = light intensities

k = Boltzmann's constant

Kn_r = Knudsen number $\equiv \lambda/R$

K_r^2 = rarefaction parameter $\equiv p_\infty R/\mu_\infty U_\infty C^*$

m = molecular mass

M = Mach number = $(2/\gamma)^{\frac{1}{2}} S$

n = number density

N = number flux to front face of cylinder

p = fluid pressure

$Q^{(2)*}(g)$ = collision integral

R = cylinder radius

Re_r = Reynolds number $\equiv \rho UR/\mu$

S = speed ratio = $U/(2kT/m)^{\frac{1}{2}}$

t = time

T = temperature

T' = potential parameter = $91.5^{o}K$

T_* = $(T_w+T_2)/2$

U = fluid velocity

$V(r)$ = intermolecular potential

(x,r) = cylindrical co-ordinates

α = power law exponent

Δt_m = time interval in simulation

λ = mean free path

μ = viscosity

ρ = fluid density

σ = potential parameter = 3.681 $\mathring{A}$

ϕ = fraction of energy exchanged in collisions

$\Omega^{(2,2)*}(T/T')$ = collision integral

Subscripts

∞ = freestream conditions

o = stagnation conditions

fm = free molecular limit

w = wall conditions

2 = conditions behind Rankine-Hugoniot shock

INTRODUCTION

One of the most successful computational methods used to predict the development of rarefied hypersonic flows has been the Monte-Carlo Direct Simulation method developed by Bird (1969, 1970a) and extended to polyatomic gases by him (1970a, 1970b) and others (e.g. Melville, 1972, Larsen and Borgnakke, 1974, Pullin, 1974, Deiwert and Yoshikawa, 1975). Diatomic collision models have been tested for hypersonic flows over a flat plate by Davis and Harvey (1976) and the calculated results were in good agreement with experiments. Agreement was not so good for the complex flow over a flat plate with forward facing step where the non-equilibrium merged layer is brought to rest (Davis and Harvey, 1979). Possible reasons for these discrepancies are errors in the experimental measurements, failure of the collision models or other aspects of the computational scheme, or the neglect of an energy transfer by vibrational relaxation in the stagnation zone.

To investigate these problems, the simpler stagnating flow ahead of a blunt cylinder has been chosen to test the accuracy of the Monte-Carlo calculations. This flow has been investigated before by Pullin, Davis and Harvey (1976) using the Monte-Carlo method. Good agreement was obtained with independent experimental measurements of heat transfer (Metcalf, Coleman and Berry, 1974). The present work compares density profiles ahead of a flat-ended cylinder, measured in a Mach 25 flow, with a new series of Monte-Carlo simulations. Heat transfer results are also compared with experimental values (Coleman, Metcalf and Berry, 1976; Doleman, 1980). Temperature profiles in the stagnation region were found to be sensitive to molecular collision model suggesting that

further experimental work to measure these profiles would allow better evaluation of the collision models.

APPLICATION OF THE DIRECT SIMULATION METHOD TO POLYATOMIC FLOWS

The collision model used to calculate the exchange of energy between translational and internal energy modes is crucial to the Monte-Carlo direct simulation method when it is extended to polyatomic gases. Three collision models have been used in the present calculations. In each the collision computation is divided into two independent parts; the calculation of scattering from intermolecular potential using monoatomic gas dynamics and the calculation of the energy exchanged between internal and external modes. The intermolecular potentials used are shown in Figure 1 compared with the Lennard-Jones potential. The three collision models used are as follows:-

(i) Inverse-power variable-ϕ model

In this model energy exchange is calculated using a modification of the restricted energy exchange method of Larsen and Borgnakke (1974). In this a fraction, ϕ, of the total centre of mass energy of collision, e_{cm}, is treated inelastically and distributed statistically amongst the translational and rotational energy modes according to an appropriate equilibrium distribution. To obtain the post-collision energies the redistributed energies are added to the fractions of each energy mode which were considered to be conserved through the collision. The variable-ϕ model is an extension to this procedure developed by Pullin (1978) and Davis (1978) whereby the fraction ϕ is not constant but is calculated for each collison as a function of e_{cm}. The functional dependence of ϕ was obtained by Pullin who derived an expression to first

order in the departure of e_{cm} from the mean value, 5kT, by relating Z_R obtained from a Chapman-Enskog transport theory calculation to the measured data of Carnevale et al (1967) for nitrogen at various temperatures. He has also shown (Pullin, 1975) that the restricted energy exchange scheme almost, but not quite, achieves detailed balance at equilibrium.

The molecular scattering is calculated using an inverse power potential, the value of the exponent, α, being chosen as 13.51 to give a temperature dependence of viscosity of $\mu \propto T^{0.648}$. The cut-off value of deflection is 0.05 radians which corresponds to a maximum value of non-dimensional impact parameter $[b(mg^2/2\alpha\beta)^{1/\alpha}]$ of 1.212. For weak collisions where the impact parameter is in the range 1.0-1.212 no exhange of rotational-translational energy is calculated.

(ii) Morse-potential, hybrid model

This model was developed by Pullin (1974) as an extension to his approximate classical calculation of energy exchange in collisions. In it, the interaction between two diatomic molecules is calculated by representing each by a rigid rotor, the force field of which consists of two short range centres of repulsion located symmetrically on the inter-nuclear axis and a weaker attractive force centred at the mid-point of the molecule. The molecules are assumed to rotate in the plane of the collision. This classical approximation was found to be unsuitable for low energy collisions and equipartition was not achieved. Hence a hybrid of classical and phenomenological methods is used. Energy exchange in high energy collisions is calculated classically while low energy collisions are treated statistically using the earlier two-class energy exchange method of Borgnakke and Larsen (1973). In this, each collision is either totally elastic or totally inelastic with probabilities $(1-\phi)$ and ϕ respectively. The value of ϕ was chosen,

and other ad hoc modifications made, in order to achieve proper relaxation behaviour.

Calculation of scattering is made according to the Morse potential

$$V(r) = 4kT'\left[\exp\left[-a(r-\sigma)\right] - \exp\left[-\frac{a}{2}(r-\sigma)\right]\right]$$

which arises in the first order perturbation solution of the equations of motion for the model molecule.

(iii) Morse-potential variable-ϕ model

This uses the Morse potential for the calculation of scattering but the hybrid calculation of energy exchange is replaced by the variable-ϕ model used with the Inverse Power model. No inelastic cut-off is applied and this, together with the slightly different collison rate produced by the Morse potential, gives a small change in relaxation behaviour.

BOUNDARY CONDITIONS

The simulation region was chosen to extend well into the undisturbed flow where molecules enter with the correct equilibrium distribution of velocity and internal energy. The downstream boundary is chosen sufficiently far away to have no effect on the flow in the stagnation region in front of the cylinder. Molecules are scattered diffusely from the body fully accommodated to the surface temperature.

NUMERICAL ACCURACY

The division of time and space into discrete intervals affects the accuracy of the simulation results. Time is divided into discrete

intervals, Δt_m, over which the molecule movement and collisions are decoupled. The flow field is divided into cells in which flow properties are considered to be constant. The general recommendations of Bird (1976) were followed when selecting cell size and Δt_m. For the lowest Knudsen number the typical cell size in the stagnation region was approximately 25% larger than the nominal freestream mean free path but less than the mean free path of emitted body particles before colliding with freestream particles. The time interval, Δt_m, was chosen as less than half the mean free time of body to freestream collisons. For Δt_m greater than this value, heat transfer results were found to increase with increasing Δt_m. Appendix A gives details of the calculation of these quantities.

A weighting factor scheme is used to keep the number of particles (and hence the number of calculated collisons) in each simulation cell approximately constant over the flow field. In these calculations weighting factors are set proportional to the radial co-ordinate of the cell centroid. As most particles are deflected away from the axis they move through a positive gradient of weighting factor.

EXPERIMENTAL PROCEDURE

Experimental data were obtained from the Imperial College Heated Nitrogen Tunnel (Harvey and Jeffery, 1971) in a Mach 25 flow. A summary of the experimental conditions is given in Table 1 where Knudsen number and Reynolds number are derived using the Lennard-Jones potential viscosity prediction (see Appendix B). A 10mm diameter flat ended cylinder, constructed from tellurium-copper, was used throughout the tests. The model was water-cooled to give measured surface temperatures of around $100^{o}C$.

Measurements were restricted to density profiles ahead of the model, normal to its surface. Density profiles, normalised against freestream density, were obtained at three different radial positions. The small size of the model precluded the use of probes to measure the flow field properties close to the body because of their disturbing influence. This made it necessary to use a non-intrusive measurement technique. The most widely used of these are the electron beam fluorescence and laser techniques. For this study the former was chosen as considerable experience has been developed at Imperial College using this method.

When a beam of electrons is fired into nitrogen gas an ultra-violet fluorescence is produced (Muntz, 1968). In gas of sufficiently low density the intensity of fluorescence is proportional to the gas density. Earlier studies (Lillicrap, 1969) have shown that good static calibrations are achieved at room or liquid nitrogen temperatures. From these it is assumed that fluorescence is independent of temperature. It is also possible to use the electron beam technique to determine rotational temperatures by analysis of the emitted spectra. However in this study the strength of the electron beam, and hence the intensity of fluorescence, was not sufficient to obtain accurate spectra and so rotational temperatures were not recorded. Heat transfer data are available from other sources whilst the questionable reliability of surface number flux measurements, due to the large corrections required, made such data unsuitable for useful comparisons with Monte-Carlo results.

The dimensions of the working section dictated that the electron gun be positioned outside the tunnel. The most convenient way to study the flowfield ahead of the model would be to fire the beam across

its face. However such an arrangement would lead to the danger of interaction between the beam and the model surface. The secondary electrons, which have a larger collision cross-section than the primaries, make an important contribution to the fluorescence. The close proximity of the model may influence the diffusion of the secondary electrons sufficiently to alter the density-intensity calibration. For this reason the electron beam was not fired across the face but instead was fired through the model from the rear, emerging from the front face normal to its surface. By doing this the distance along the beam path close to the model was reduced thus minimizing the risk of distortion of the electron cloud. The diameter of the beam guide through the model was 0.5mm. The electron beam was fired radially towards the axis where it was magnetically deflected through 90^{o} to pass through the model (Figure 3). Although the bending gave rise to some electron scattering, the collimating effect of the hole through the model resulted in a fine near parallel beam emerging from the model face.

The model used in these tests consisted of a cylindrical core, through which the electron beam was guided, and an eccentric outer ring which could be rotated to move the axis of the model relative to the electron beam axis (Figure 5a). The model contained a cavity which was pressurised to balance the surface pressure thus preventing flow along the beam guide hole (Figure 5b). Surface temperature was measured with a thermocouple set into the model face. The axis of the model was set 9mm below the tunnel axis to avoid any flow disturbance that might focus there.

Density profiles were obtained by measuring the total intensity of the [0-0] band of the $N_2^+(1-)$ system of the nitrogen spectrum using a photomultiplier with suitable optical filtering. The photomultiplier was linked to an optical traverse by a fibre-optic cable and the beam

image was focused onto a slit 0.15mm wide using a quartz lens. Fluctuations of the intensity due to changes in the beam current were monitored using a second, similar optical and photomultiplier arrangement focused at a fixed point on the beam axis ahead of the disturbed flow.

For each traverse from the model surface, forward from the model surface through the shocklayer into the freestream, the motion was stopped at about twenty points. Each position was held for long enough to ensure that measurements were unaffected by the response of the filters included in the photomultiplier amplifiers to reduce noise. Whilst the traverse was moved from one position to the next, the field strength of the beam deflection magnet was altered sufficiently to prevent the electron beam passing through the model thus enabling measurements to be made of stray background light. The continuous outputs from the two photomultipliers and from the traverse position transducer were recorded digitally using the laboratory's high speed data acquisition system. The beam intensity at each position, after corrections for the background light level and fluctuations of beam intensity were made, was normalised against freestream intensity. Very close to the model surface the optical path was partially obscured which gave falsely low light intensity measurements. Compensation was made using a cut-off calibration which was recorded with no flow (Figure 4).

FLOW FIELD DESCRIPTION - SIMULATION RESULTS

Calculations have been made using the Morse-potential variable-ϕ model for a range of Knudsen number (see Table 2) extending from near the free molecular limit to conditions typical of those produced in the nitrogen tunnel. Near axis profiles of density, x-velocity, translational and rotational temperature are shown in Figures 6-8.

Included for comparison is an approximate inviscid solution based on the shock stand off distance calculated by Vinokur (1959) and the Rankine-Hugoniot normal shock for an inviscid non-conducting gas. These profiles are qualitatively similar to those calculated for a Mach 10 flow by Pullin et al (1976).

The temperature disturbance extends further from the body than the density disturbance over the whole range of Knudsen number. Density rises gently to approximately the inviscid value near the free molecular limit to more than twice this value at the lower Knudsen numbers. Translational temperature jumps suddenly for lower Knudsen numbers, the peak value occurring where the density has only risen to a small fraction of its near body peak value. In the denser flows, translational temperature overshoots the value behind the equivalent continuum shock and approaches the value for frozen rotational modes ($\gamma = 1.67$). The rotational temperature lags and never reaches the inviscid value. After the temperature jump, translational and rotational temperatures are bought towards equilibrium by collisions with body emitted particles. The temperature profiles can be extrapolated reasonably well towards equilibrium near the wall temperature, although it is a characteristic of the energy exchange models that equipartition is never exactly achieved.

Contours of density and speed for conditions similar to those in the experiments are shown in Figures 9 and 10. The radial gradients of density $\partial\rho/\partial r$ are very small for most of the region in front of the body. The position of the peak translational temperature is also shown in Figure 9. The temperature peak occurs where the density ratio is approximately 2.0 - 3.0.

To check if vibrational relaxation could be affecting the experimental results near the stagnation line, collision rates were estimated from the simulation results. This estimate depends on the cut-off conditions used in the collision model for the simulation.

The cut-off condition for the Morse potential has been chosen to include all those collisions which result in an appreciable molecule trajectory deflection or transfer of rotational energy (Pullin, 1974). Hence a collision likely to release vibrational energy would also be included. Figure 11 shows streamlines derived from the simulation and the approximate accumulative number of collisions for a molecule travelling along the streamlines. The expected number of collisions for a molecule travelling through the "shock" and along the front face of the cylinder is approximately 2000. The vibrational collision number at the stagnation temperature of these experiments (1200-2000^{o}K) is approximately 10^5 (Vincenti and Kruger, 1965). Hence vibrational energy is essentially frozen and the flow may be simulated by the present models which ignore vibrational energy.

COMPARISON WITH EXPERIMENTS

Two sets of flow conditions were chosen for detailed comparison of simulation with experimental results. Table 3 shows the flow conditions and the range of experimental runs matching these conditions. Because of the cell arrangement used in the calculations, flow properties cannot be obtained at the axis. As the radial gradients are small near the axis flow properties at r/R = 0.05 have been taken as stagnation line values.

Figures 12(a) and 12(b) show the temperature profiles obtained using the various collision models. The position of the peak of translational temperature is similar for each model but the rotational temperature profiles are slightly different. The classical calculation of energy exchange (used in the hybrid model) forces the rotational temperature towards equilibrium with the translational temperature more

rapidly than does the variable-ϕ calculation. The hybrid model produces an overshoot of rotational temperature whereas the variable-ϕ models approach equilibrium with rotational temperature below translational temperature. Figure 12(a) shows an increased scatter in translational temperature near the freestream for the hybrid model. The samples sizes for these cells are much smaller than those where density is greatest and this, coupled with the small number of collisions calculated in these cells, produces this effect. There also appears to be a general increase in scatter for samples near the axis, an effect possibly arising from the radial weighting factor scheme.

Figures 13 and 14 show experimental stagnation line density profiles compared with the simulation results. Included on these figures are the temperature profiles for the Morse-potential variable-ϕ model which can be taken as typical of the three models. The extent of the density disturbance and the near wall values are well predicted by each collision model. Between these limits the prediction is not quite so good. There appears to be a kink in the simulation profiles at about $x/R = -0.25$. This effect was also reported in the Monte-Carlo calculations of Pullin et al (1976) where it was suggested that it was the beginning of the formation of a merged shock layer. The kink does not coincide with the sharp rise in temperature and is unlikely to be anything other than a result of statistical scatter in the complex region of the flow after the temperature rise. In this region where stream particles are colliding with emitted body particles there is a large exchange of rotational and translational energy and any errors in the collision models would tend to be exaggerated. It could also be another demonstration of the increased scatter near the axis as the effect is reduced at greater radial distance from the axis (see Figure 15) and is almost gone at $r/R = 0.85$ (Figure 16).

There is a slight tendency for the simulations to underestimate the near wall density towards the edge of the face of the cylinder. The experimental density profiles of Figures 17(a) and 17(b) show very little variation with Knudsen number or radial distance from the axis. The radial density distributions of Figure 18 and the density contours of Figure 9 show that the near wall density value decreasing slightly away from the axis.

It is not possible to choose the best collision model from these results. Each model shows the same deviations from the experimental data. All three models give reasonable density predictions and any variations could easily be the results of statistical scatter.

HEAT TRANSFER

Heat transfer to the body has been calculated and expressed as Stanton number, i.e.

$$C_h = \frac{\dot{q}}{\rho_\infty U_\infty (H_o - H_w)} \doteq \frac{\dot{q}}{\frac{1}{2}\rho_\infty U_\infty^3 (1 - T_w/T_o)} .$$

The free molecular limit for a diffusely reflecting surface (see Bird, 1976) can be expressed as

$$C_{hfm} \doteq \frac{1 + \frac{\gamma}{S_\infty^2 (\gamma-1)} - \frac{\gamma+1}{2}\left(\frac{1}{(\gamma-1)S_\infty^2} + \frac{1}{\gamma}\right)\frac{T_w}{T_o}}{(1 - T_w/T_o)} .$$

The heat transfer distribution across the front face of the cylinder using the Morse potential, variable ϕ model, for various Knudsen numbers is shown in Figure 19. The flow conditions are those in Table 2. For the most rarefied conditions the heat transfer is

virtually uniform despite the scatter, but still below the free molecular limit. As the flow density increases the total heat transfer falls and the distribution approaches the shape of the inviscid predictions of Vinokur (1962).

To correlate the heat transfer results for different Mach numbers, stagnation temperatures and wall temperatures we have followed Metcalf et al (1976) in using Cheng's (1961) rarefaction parameter, K_r^2, defined by

$$K_r^2 = \frac{p_\infty R}{\mu_\infty U_\infty C^*} \quad ,$$

where $$C^* = \frac{\mu^* T_\infty}{\mu_\infty T^*} \quad .$$

T^* is a reference temperature behind the nominal shock and μ^* is the viscosity at this temperature. The reference temperature is taken as $\frac{1}{2}(T_2 + T_w)$.

The rarefaction parameter K_r^2 may be expressed as

$$K_r^2 = \frac{n_\infty k T^* R}{U_\infty \mu^*} \quad .$$

The parameter is relatively insensitive to the viscosity prediction used since most viscosity formulations agree closely at the high reference temperature (see Figure 2).

Alternatively, K_r^2 may be calculated from Knudsen number using the relation

$$K_r^2 = \frac{8(\frac{2}{\gamma \pi})^{\frac{1}{2}}}{5 M_\infty C^* Kn_{r,\infty}} \quad ,$$

where $$C^* = \frac{\Omega^{(2,2)*}(T_\infty/T')T_\infty^{\frac{1}{2}}}{\Omega^{(2,2)*}(T^*/T')T_*^{\frac{1}{2}}} \quad ,$$

and $\Omega^{(2,2)*}(T/T')$ is the collision integral used to define $Kn_{r,\infty}$ (see Appendix B).

Figure 20 shows heat transfer distributions across the face and along the side of the cylinder for different values of K_r^2. These were calculated using the Morse and inverse power potentials and the variable-ϕ energy exchange. The average heat transfer to the front face of the cylinder for various flow conditions is plotted against K_r^2 in Figure 21. A summary of the Monte-Carlo results on this graph is shown in Table 4 including the results of Pullin et al (1976) taken from a similar graph in that paper. These are plotted against K_r^2 as calculated in this paper. The experimental results of Coleman, Metcalf and Berry (1976) and Doleman (1980) are also shown. The experimental results have been converted from stagnation point values to average front face values using the relationship defined in the earlier paper of Metcalf, Coleman and Berry (1974).

The Monte-Carlo results are well correlated by the parameter K_r^2 and the fit with experimental data is good in the range $0.1 < K_r^2 < 2.0$. Near the molecular limit the simulation results are lower than the experimental values while near the continuum they are higher. The three collision models give different values of heat transfer for the same condition. The spread of the data on Figure 21 does not allow us to choose the best model. The differences in temperature profiles produced by each model might allow such a choice to be made. Figures 22(a) and (b) show stagnation line temperature profiles for two different flow conditions. Translational and rotational temperature profiles are those from Figures 12(a) and (b) and the badly scattered data for the hybrid model in one case has been "averaged" to give a smooth temperature profile before the temperature jump. Also included is the radial component of translational temperature as

predicted by each model. The difference in heat transfer predictions for each model is primarily a result of the different proportion of translational energy which is directed parallel to the body surface and thus away from the body. The number flux to the total front face of the model is shown with the radial component of translational temperature for each model. The harder inverse power potential deflects more of the freestream energy radially and the number flux and heat transfer are correspondingly lower. The classical calculation of energy exchange in the hybrid model gives a smaller component of radial temperature than the variable ϕ calculation for the same Morse potential possibly because a greater proportion of collisions are calculated at lower relative velocity when the attractive component of the Morse potential produces smaller deflections.

SUMMARY AND CONCLUSIONS

The Monte-Carlo direct simulation technique has been shown to give good predictions of density in the stagnation flow in front of a flat-faced cylinder. Three collision models have been tested and all were found to be in good agreement with experimentally determined density profiles. Heat transfer predictions, though showing a variation with collision model, were in reasonable agreement with experiment. The combined effects of scatter in the Monte-Carlo density profiles and the spread of heat transfer data make it impossible to determine the most accurate collisional model from these calculations. There are, however, significant differences in temperature profiles predicted for each collisional model. Good experimental profiles for one or more of the temperature components should provide clear evidence of which model is more precise. Unfortunately such data could not be obtained in the present experiments.

APPENDIX A

Mean free path of emitted body molecules in rarefied flow - λ_w

The mean free path of molecules emitted from the surface of a body before colliding with molecules incident to the body, λ_w, can be approximated for hard sphere molecules by

$$\lambda_w = \frac{3/4}{n_\infty d^2 (S_\infty (\pi T_\infty / T_w)^{\frac{1}{2}} + 1)}$$

(Whitfield, 1973).

The corresponding mean free time is

$$t_w = \lambda_w / \bar{c}_w \ .$$

blunt body

This is derived for ~~flat plate flow~~ where the angle β between the freestream velocity and the normal to the surface is 90^o. 0^o

To account for different surface orientations an approximate method may be used:

$$\lambda_w = \frac{1}{n_\infty A(g)\ S_\infty (T_\infty / T_w)^{\frac{1}{2}}}$$

where A(g) is the collision cross-section at relative speed of collision, g, given by

$$A(g) = \pi \sigma^2 Q^{(2)*}(g)$$

Values of the collision integral $Q^{(2)*}(g)$ used were those calculated by Pullin (1974) for the Morse potential. The relative velocity, g,

between freestream and body emitted particles is given by

$$g = \left(\left(U_\infty + \bar{c}_w \cos\beta\right)^2 + \left(\bar{c}_w \sin\beta\right)^2 \right)^{\frac{1}{2}} .$$

A further refinement is to calculate A(g) as the weighted average value for a representative sample of collisions between body emitted particles and freestream particles, each selected by a Monte-Carlo procedure from the appropriate distribution.

In these calculations the hard sphere value of λ_w was approximately 80% of that calculated for the Morse potential. The hard sphere values of t_w and λ_w were used to set Δt_m and cell sizes.

APPENDIX B

Flow Parameters

The following parameters are used:-

$$\text{Reynolds Number,} \quad Re_{r,\infty} = \frac{\rho_\infty U_\infty R}{\mu_\infty} \ ,$$

where μ_∞ is calculated from the Chapman-Enskog formulation of viscosity using the Lennard Jones potential i.e.

$$\mu_\infty = \frac{5(\pi m k T_\infty)^{\frac{1}{2}}}{16\pi\ \sigma^2\ \Omega^{(2,2)*}(T_\infty/T')} \ .$$

T' and σ are potential parameters chosen to match experimental viscosity data. Values of the collison integral are taken from Monchick and Mason (1961) where T' = 91.5^{o}K and σ = 3.681 $\mathring{A}$. The viscosity prediction (Figure 2) using the Lennard-Jones potential differs by less than 2% from those quoted by NACA (Woolley, 1956) where a value of T' = 91.46^{o}K was used.

A nominal mean free path in a frame of reference moving with the freestream may be defined from the Chapman-Enskog derived relation

$$\mu = \frac{5\pi}{32} \rho \bar{c} \lambda \ .$$

Hence

$$\lambda_\infty = \frac{1}{\sqrt{2}\pi\ \sigma^2 n_\infty \Omega^{(2,2)*}(T_\infty/T')} \ ,$$

The Knudsen numberand Reynolds number are related by

$$Kn_{r,\infty} = \frac{32\ (\gamma/2\pi)^{\frac{1}{2}}\ M_\infty}{10\ Re_{r,\infty}} \ .$$

TABLE 1: EXPERIMENTAL CONDITIONS

Run No.	P_o (MN/m^2)	T_o (°K)	M_∞	T_w (°K)	$Kn_{r,\infty}$	$Re_{r,\infty}$
9613	5.570	2221	25.19	392	.1018	374
9615	5.470	2320	25.16	397	.1095	347
9603	6.216	1604	26.01	368	.0676	581
9604	6.214	1603	26.05	369	.0681	578
9722	6.606	1236	25.87	362	.0442	884
9723	6.577	1264	25.91	363	.0460	851
9724	6.536	1305	25.79	366	.0473	824
9591	4.826	1366	24.83	362	.0577	650
9592	4.822	1371	24.83	363	.0573	655
9593	4.814	1382	24.60	364	.0564	659
9596	4.735	1482	24.30	375	.0596	616
9631	4.887	1295	25.77	359	.0624	624
9633	4.896	1282	25.77	360	.0615	633
9634	4.890	1291	25.68	360	.0612	634
9636	4.765	1453	25.20	373	.0675	564
9693	4.785	1423	25.77	363	.0721	540
9694	4.759	1455	25.76	365	.0745	522
9695	4.714	1513	25.76	370	.0789	493
9704	3.770	1497	25.66	353	.0960	404
9705	3.776	1488	25.56	353	.0935	413
9576	3.791	1460	25.31	354	.0871	439
9577	3.831	1395	25.24	354	.0802	481
9597	4.618	1629	24.33	386	.0697	527
9598	4.603	1648	24.54	391	.0737	503
9596	4.607	1647	25.40	376	.0853	450

MODEL RADIUS R = 5mm

T A B L E 2

T_o (°K)	M_∞	T_w (°K)	$Kn_{r,\infty}$	$Re_{r,\infty}$
1446	24.77	375	1.840	20
			1.382	27
			0.613	61
			0.306	122
			0.0656	570
			0.0465	805

T A B L E 3 AVERAGE MATCHING CONDITIONS (M-C CALCULATIONS)

Run Nos.	P_o (MN/m^2)	T_o (°K)	M_∞	T_w (°K)	$Kn_{r,\infty}$	$Re_{r,\infty}$
9613 9615	5.520	2271	25.17	396	.1056	360
9591 to 9695	4.816	1383	25.40	363.5	.0648	592

T A B L E 4: HEAT TRANSFER

M_∞	T_o (°K)	T_2 (°K)	T_w (°K)	T^* (°K)	C_{hfm}	$Kn_{r,\infty}$	K_r^2	C_{hav}	Potential	Energy exchange	Source
24.77	1446	1405	375	890	1.058	1.840	.045	.887	Morse	var ϕ	
						"	"	.885	Inv.pow.	var ϕ	
						1.382	.060	.868	Morse	var ϕ	
						"	"	.872	Morse	hybrid	
						.613	.136	.768	Morse	var ϕ	
						.306	.271	.670	"	"	
						.0656	1.27	.424	"	"	present
						.0465	1.79	.364	"	"	
25.40	1383	1344	364	854	1.059	.0648	1.25	.474	Morse	hybrid	
						"	"	.405	Morse	var ϕ	
						"	"	.385	Inv.pow.	var ϕ	
25.17	2271	2207	396	1301	1.038	.1603	.84	.558	Morse	hybrid	
								.521	Morse	var ϕ	
								.450	Inv.pow.	var ϕ	
10.0	2000	1941	300	1120	1.077	7.66	.025	.93	Inv.pow.	ϕ =0.1	
						2.30	.083	.84	"	"	
						.766	.25	.72	"	"	Pullin et al
						.383	.50	.55	"	"	(1976)
						.128	1.50	.40	"	"	
						.0383	5.00	.30	"	"	

REFERENCES

BIRD, G.A.

- "Direct Simulation Monte Carlo Method - Current States and Prospects", Rarefield Gas Dynamics (ed. Trilling and Wackman, 6th Symposium (1969).
- "Numerical Simulation of the Boltzmann Equation", Rarefied Gas Dynamics, (ed. Dini), 7th Symposium (1970a).
- "Breakdown of Translational and Rotational Equilibrium in Gaseous Expansions", AIAA Jour., Vol. 8, No. 11, p.1998 (1970b).
- "Molecular Gas Dynamics", Oxford (1976).

BORGNAKKE, C., and Larsen, P.S., "Statistical Collision Model for Monte Carlo Simulation of Polyatomic Gas", Dept. of Fluid Mechanics, Technical University of Denmark, Lyngby, Denmark, AFM 73-08 (1973).

CARNEVALE, E.H., Carey, C., and Larsen, G., "Ultrasonic Determination of Rotational Collision Numbers and Vibrational Relaxation Times of Polyatomic Gases at High Temperatures", J. Chem. Phys., Vol. 47, No. 8, p.2829 (1967).

CHENG, H.K., "Hypersonic Shock-Layer Theory of the Stagnation Region at Low Reynolds Number", in Proc. of the 1961 Heat Transfer and Fluid Mechanics Institute (1961).

COLEMAN, G.T., Metcalf, S.C., and Berry, C.J., "Heat transfer to Hemisphere Cylinders and Bluff Cylinders Between Continuum and Free Molecular Limits", Rarefied Gas Dynamics, (ed. Potter), 10th Symposium (1976).

DAVIS, J., "An Experimental Study to Evaluate and Develop the Direct Simulation Method as Applied to Rarefied Hypersonic Flow Fields", Dept. of Aero., Imperial College, Ph.D. Thesis (1978).

DAVIS, J., and Harvey, J.K.

- "Comparison of the Direct Simulation Method with Experiment for Rarefied Flat Plate Flow", Rarefied Gas Dynamics, (ed. Potter) 10th Symposium (1976).

- "Experimental Studies Using a Hollow Cylinder to Evaluate the Collision Kernels for Monte-Carlo Calculation", Rarefied Gas Dynamics, (ed. Campargue), 11th Symposium (1979).

DEIWERT, G.S., and Yoshikawa, K.K., "Analysis of a Semiclassical Model for Rotational Transition Probabilites", Phys. of Fluids, Vol. 18, No. 9, p.1085 (1975).

DOLEMAN, K.A., "Heat Transfer to a Hemisphere-Cylinder and a Bluff Cylinder in High Altitude Flight", R.A.E., Tech. Memo. Aero. 1819 (1980).

HARVEY, J.K., and Jeffery, R.W., "The Imperial College Graphite Heated Hypersonic Wind Tunnel", Dept. of Aero., Imperial College, Rep. No. 71-01 (1971).

LARSEN, P.I., and Borgnakke, C., "Statistical Collision Model for Simulating Polyatomic Gas with Restricted Energy Exchange", Rarefied Gas Dynamics, (ed. Becker, Fiebig) 9th Symposium (1974).

LILLICRAP, D.C., "A Study of Rarefied Flows using an Electron Beam", Dept. of Aero., Imperial College, Ph.D. Thesis (1969).

MELVILLE, W.K., "The Use of the Loaded Sphere Molecule Model for Computer Simulation of Diatomic Gases", J. Fluid Mech., Vol. 51, Part 3, p.571 (1972).

METCALF, S.C., Coleman, G.T., and Berry, C.J., "Heat transfer to Bluff Faced and Hemispherical Faced Cylinders between Continuum and Free Molecular Limits", Rarefied Gas Dynamics (ed. Becker, Fiebig) 9th Symposium (1974).

MONCHICK, L., and Mason, E.A., "Transport Properties of Polar Gases", J. Chem. Phys., Vol. 35, No. 5, p.1676 (1961).

MUNTZ, E.P., "The Electron Beam Fluorescence Technique" AGARDograph 132 (1968).

PULLIN, D.I.,

- "Rarefied Leading Edge Flow of a Diatomic Gas", Dept. of Aero., Imperial College, Ph.D. Thesis (1974).
- "Model Kinetic Equations for Structureless Polyatomic Molecules with Phenomenological Energy Exchange", Dept. of Aero., Rep. No. 75-10 (1975).
- "Kinetic Models for Polyatomic Molecules with Phenomenolgical Energy Exchange", Phys. of Fluids, Vol. 21, p.209 (1978).

PULLIN, D.I., Davis, J., and Harvey, J.K., "Monte-Carlo Calculations of Axisymmetric Rarefied Transition Flow Past a Bluff-Faced Cylinder", Rarefied Gas Dynamics, (ed. Potter), 10th Symposium (1976).

VINCENTI, W.G., and Kruger, C.H., "An Introduction to Physical Gas Dynamics", Wiley, N.Y., Chap. VII , Section 2 (1965).

VINOKUR, M.,

- "Hypersonic Flow Around Bodies of Revolution which are Generated by Conic Sections", 6th Midwestern Conference on Fluid Mechanics, Uni. of Texas (1959).

- "Laminar Heat-Transfer Distribution on Oblate Ellipsodial Noses in Hypersonic Flow", J. Aerospace Sciences, Vol. 29, p.113 (1962).

WHITFIELD, D.L., "Mean Free Path of Emitted Molecules and Correlation of Sphere Drag Data", AIAA Jour., Vol. 11, No. 12, p.1666 (1973).

Woolley,H.W., "Thermodynamic Properties of Gaseous Nitrogen", NACA TN 3271 (1956).

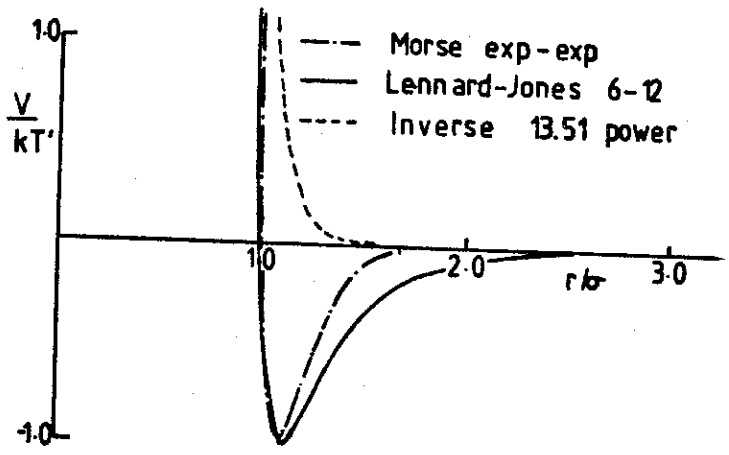

Inter-molecular potential

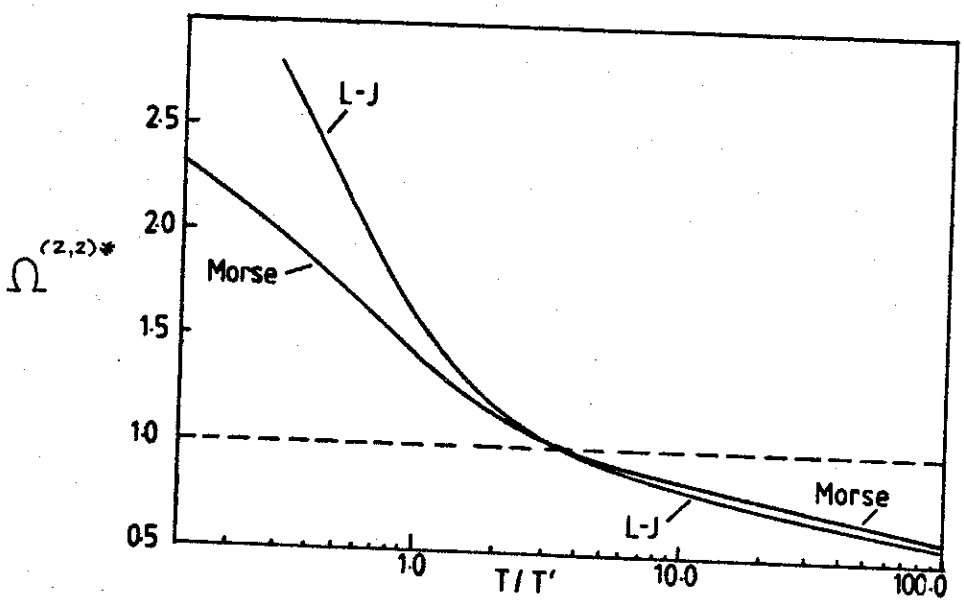

Reduced collision integral

Fig. 1 Comparison of potentials
(after Pullin, 1974)

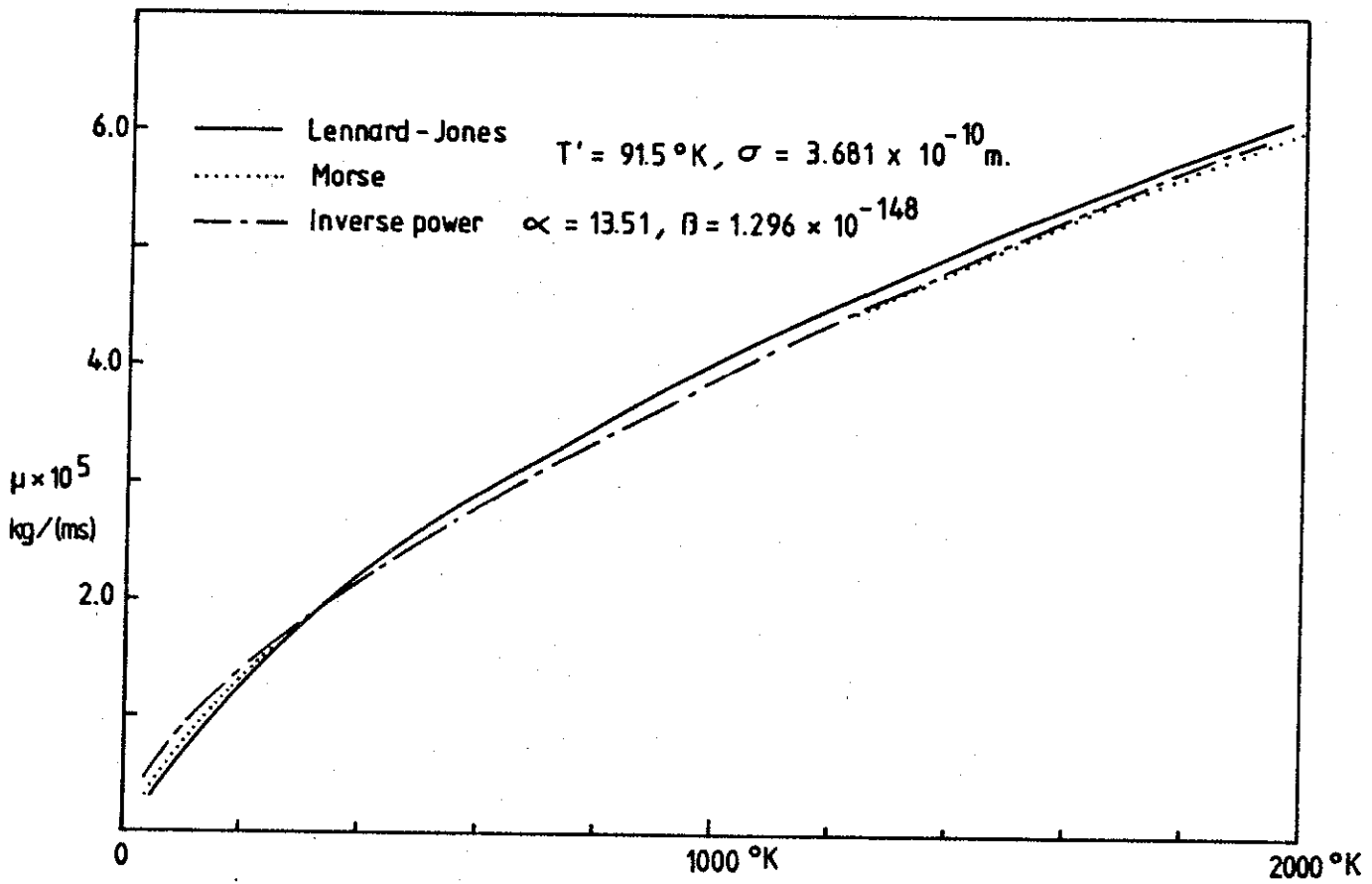

Fig. 2 VISCOSITY of N_2

(predictions for different inter-molecular potentials)

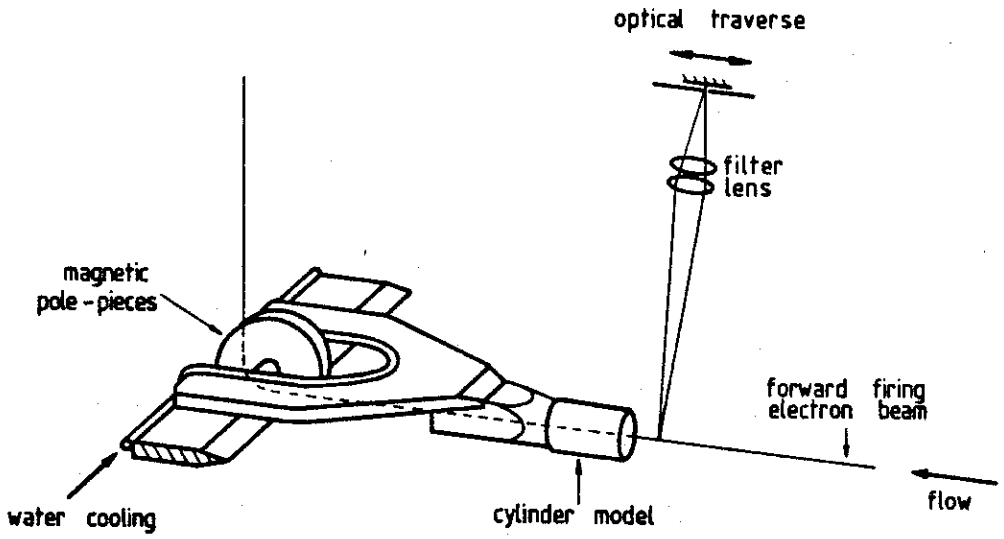
optical traverse
filter
lens
magnetic
pole-pieces
forward firing
electron beam
flow
water cooling
cylinder model

Fig.3

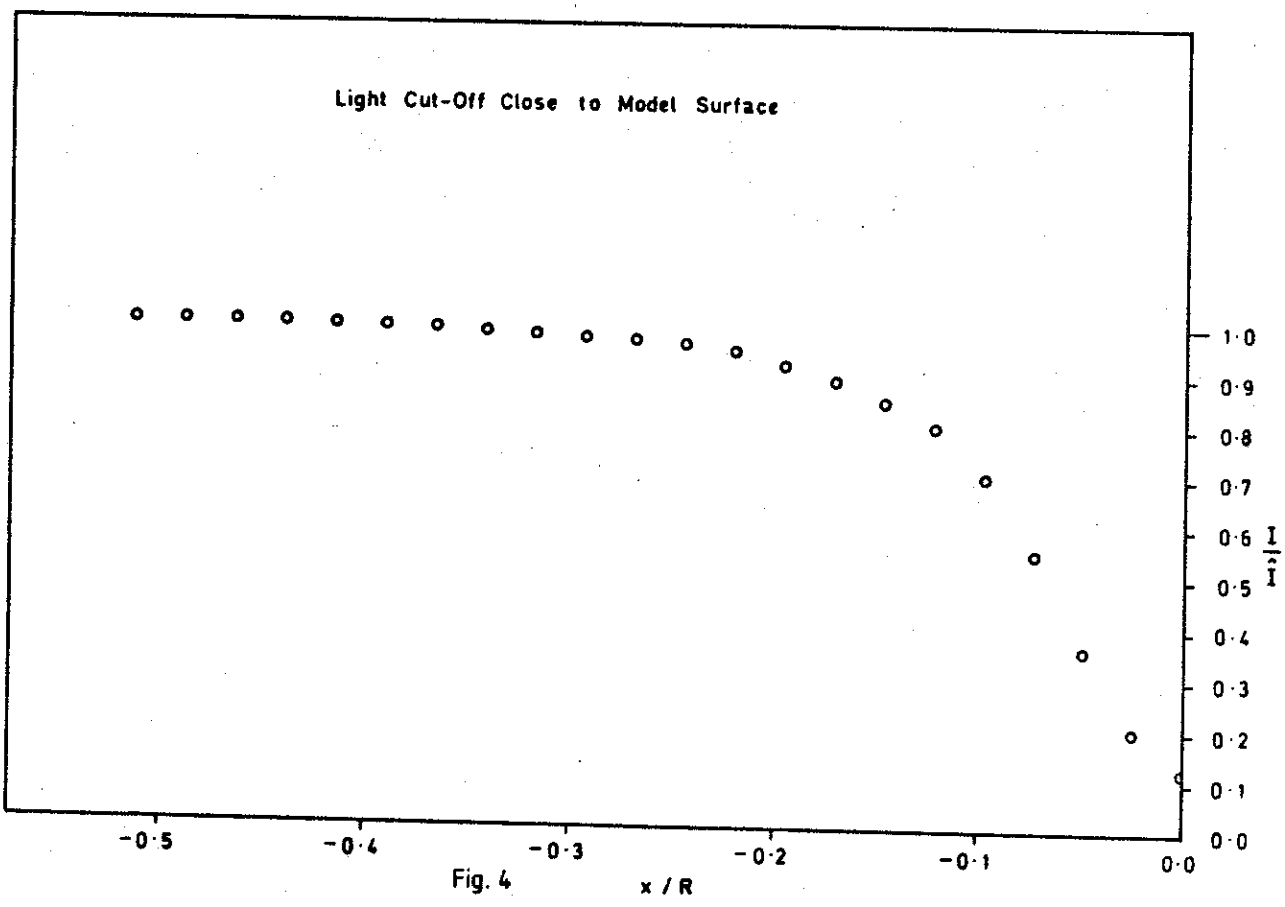
Light Cut-Off Close to Model Surface
1·0
0·9
0·8
0·7
0·6
0·5
0·4
0·3
0·2
0·1
0·0
I/Î
-0·5
-0·4
-0·3
-0·2
-0·1
0·0
x / R

Fig. 4

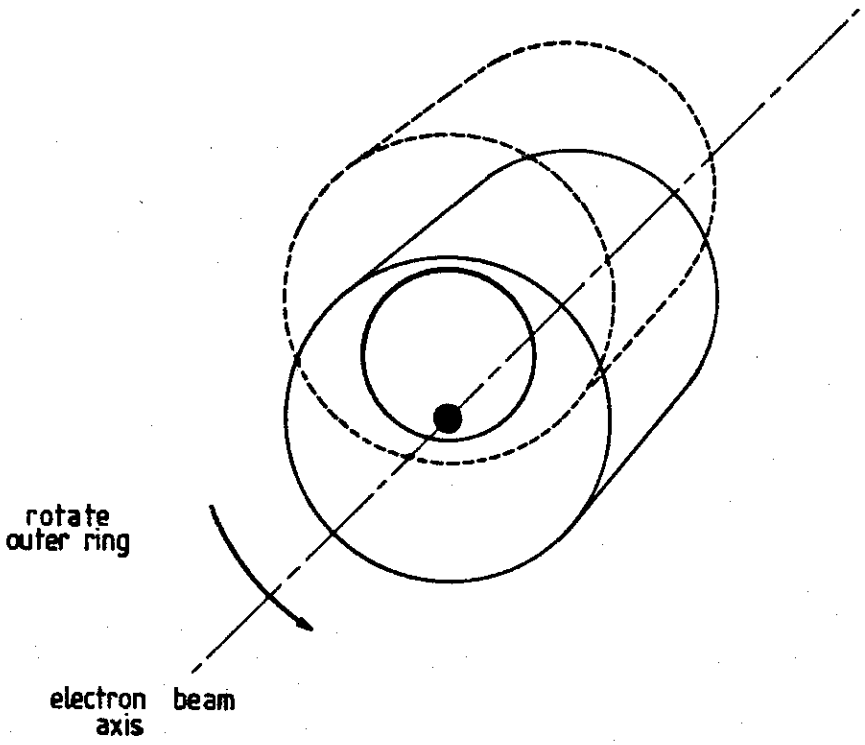
rotate
outer ring
electron beam
axis

Fig. 5a

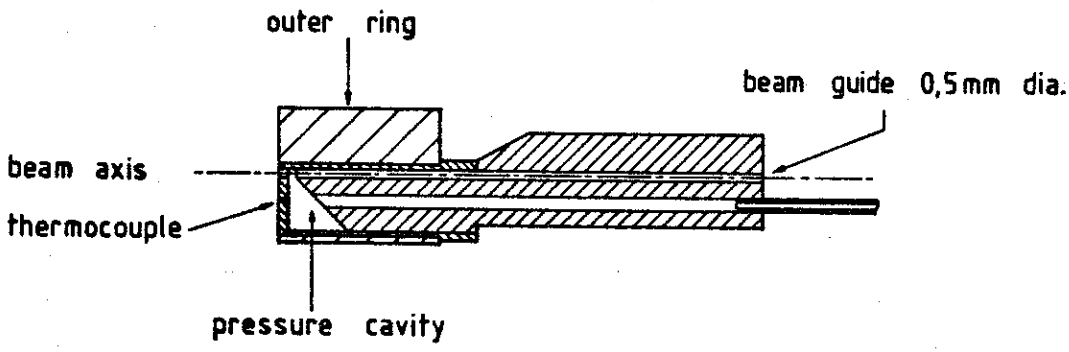
outer ring
beam guide 0,5mm dia.
beam axis
thermocouple
pressure cavity

Fig. 5b

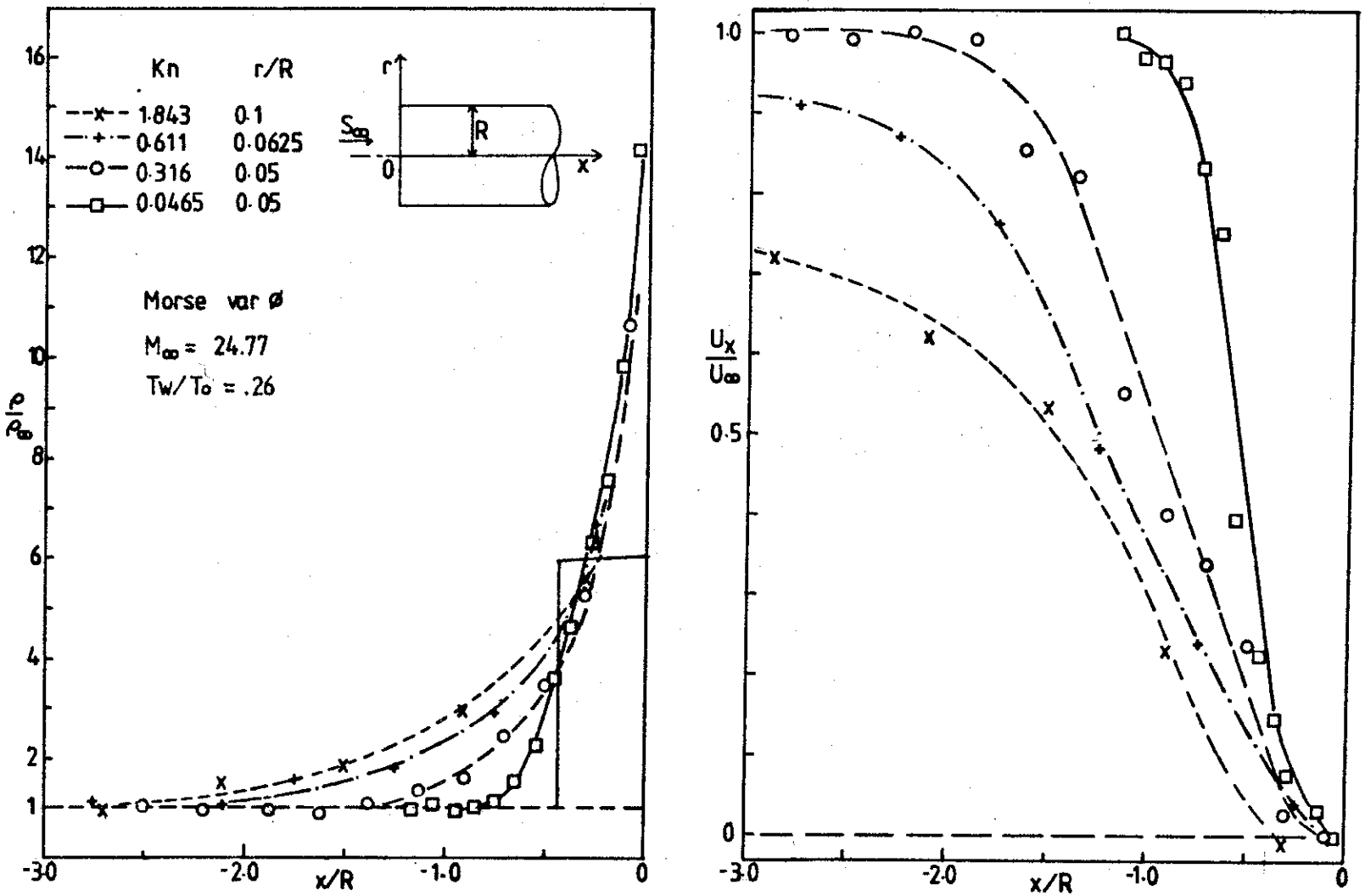

Fig. 6 Near axis density and x-velocity profiles

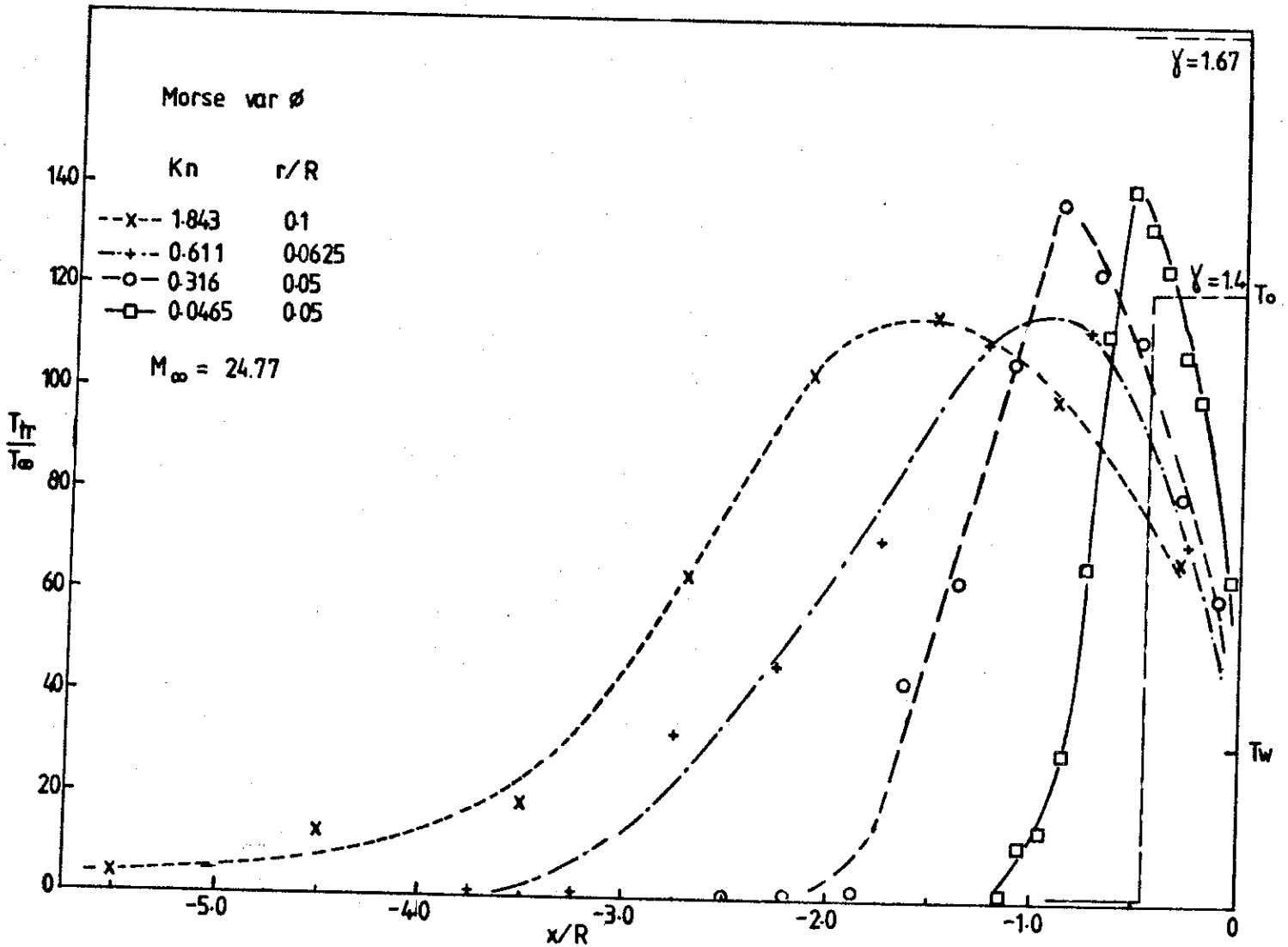

Fig.7 Near axis translational temperature profiles

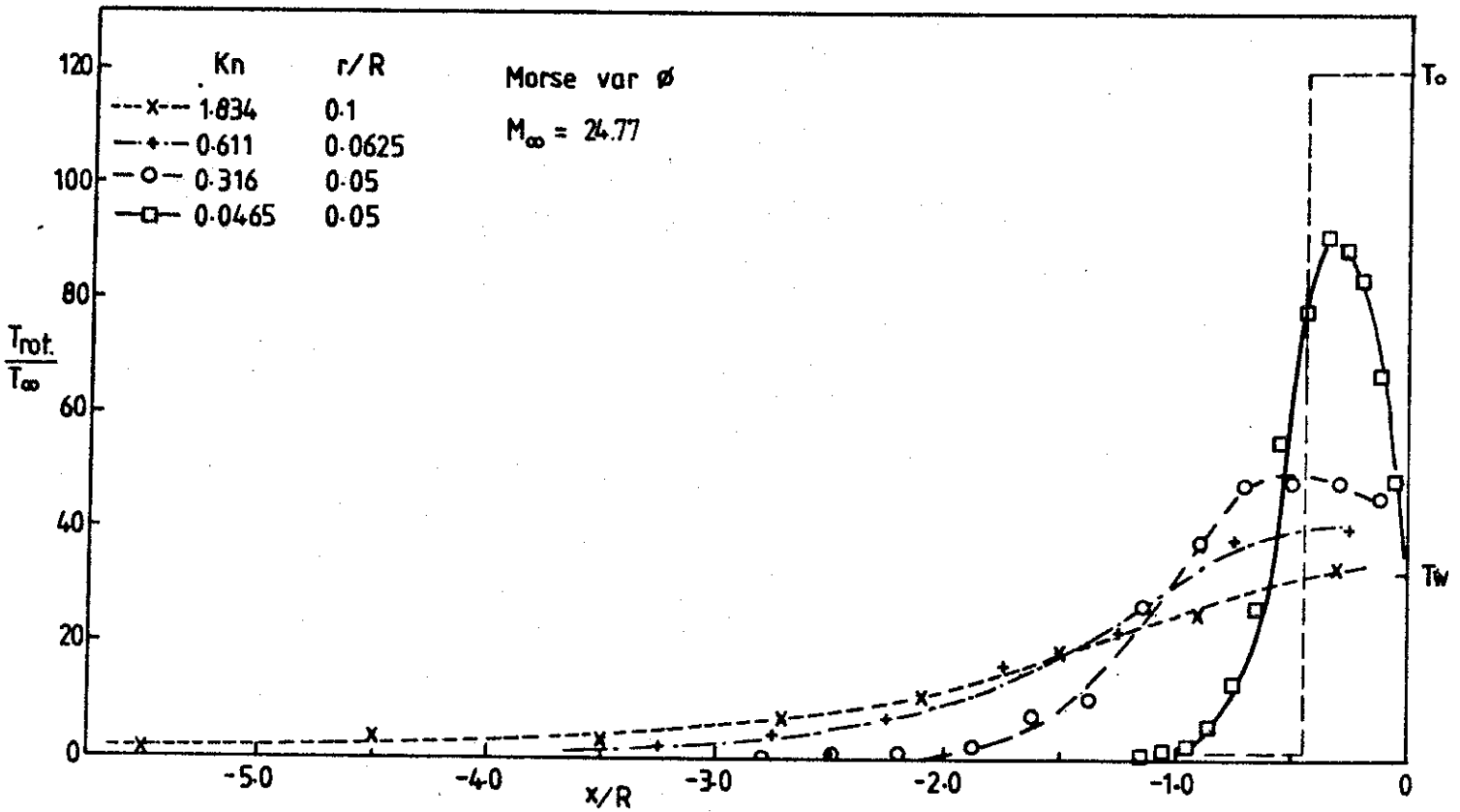

Fig. 8 Near axis rotational temperature profiles

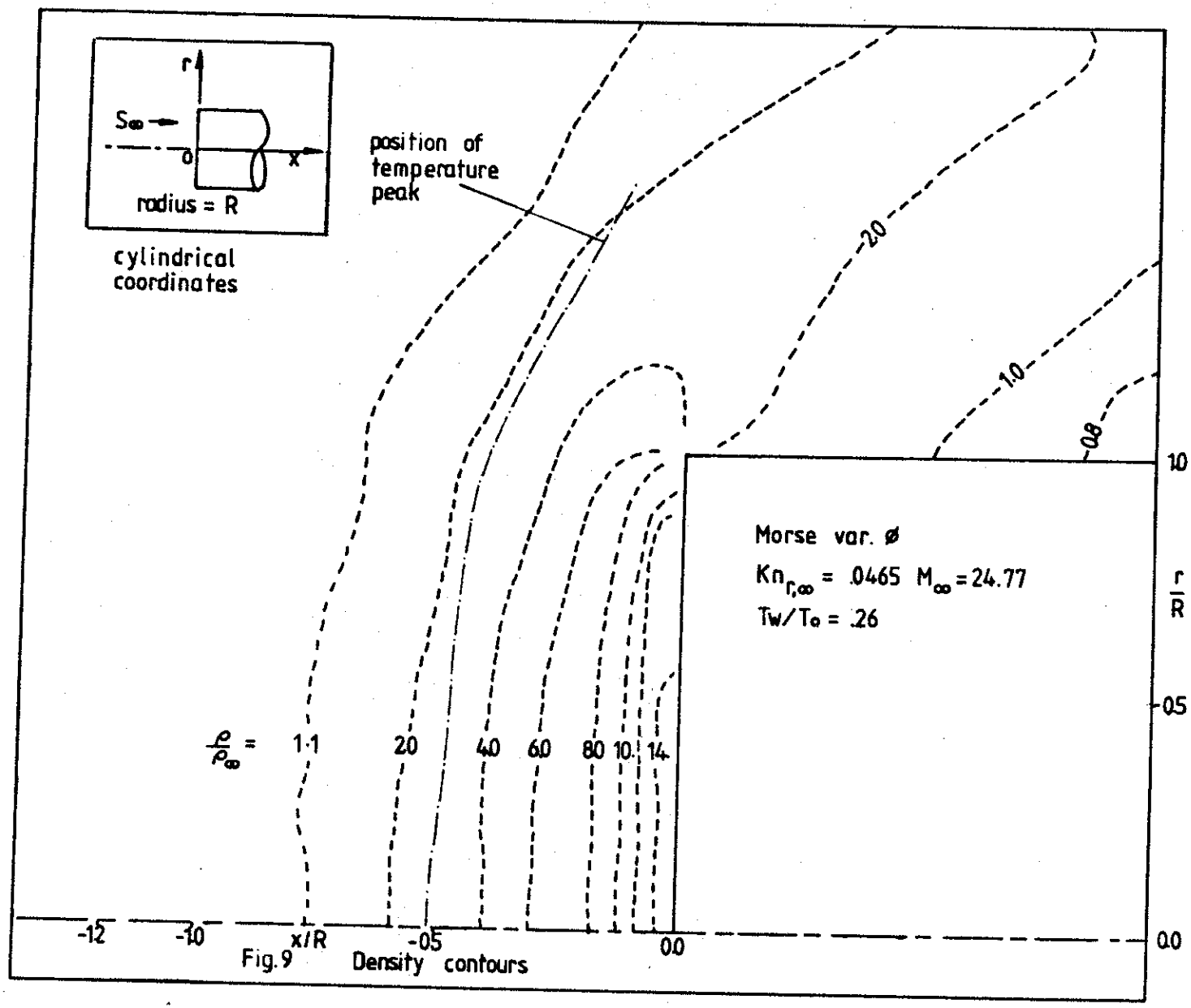

Fig. 9 Density contours

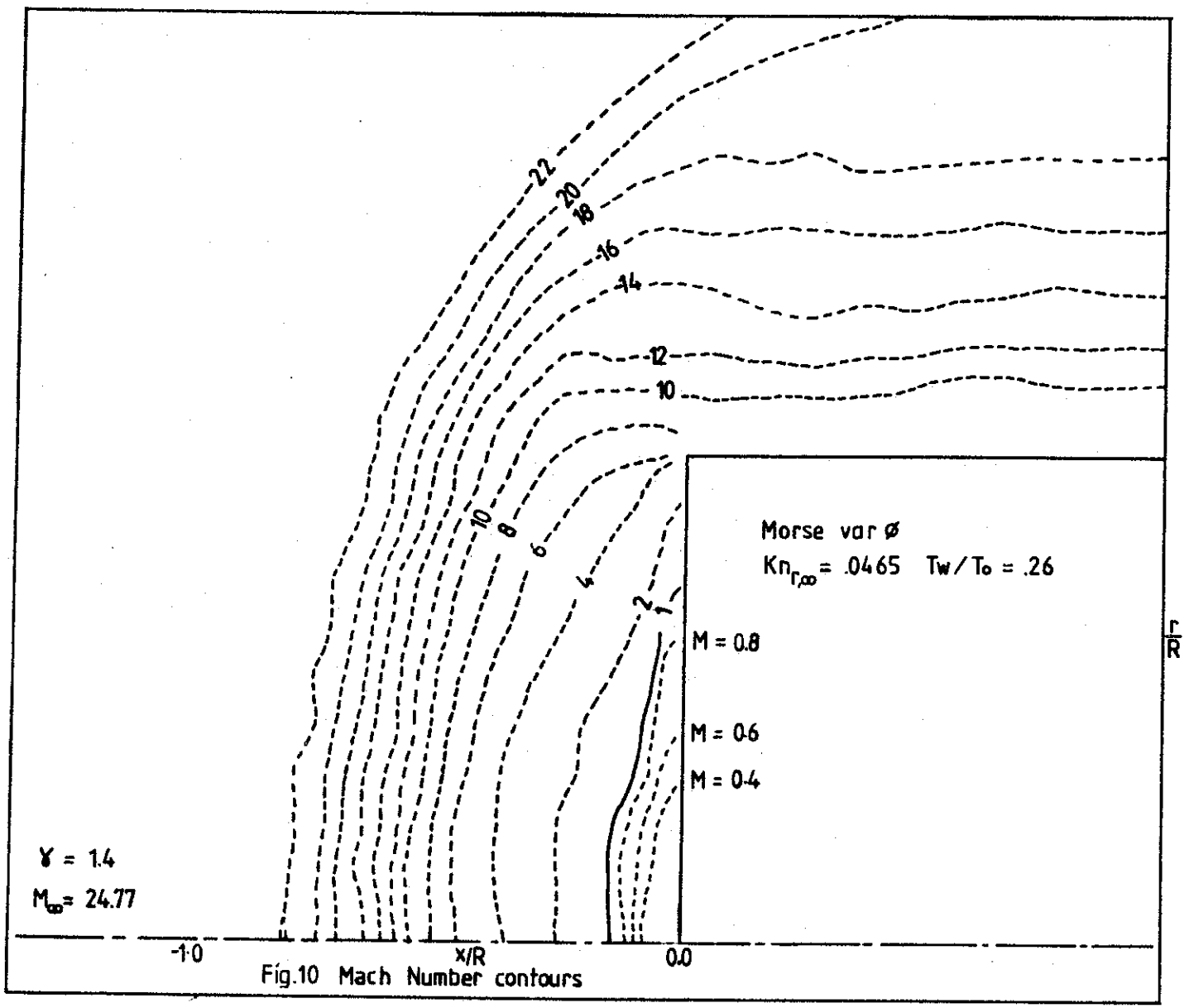

Fig.10 Mach Number contours

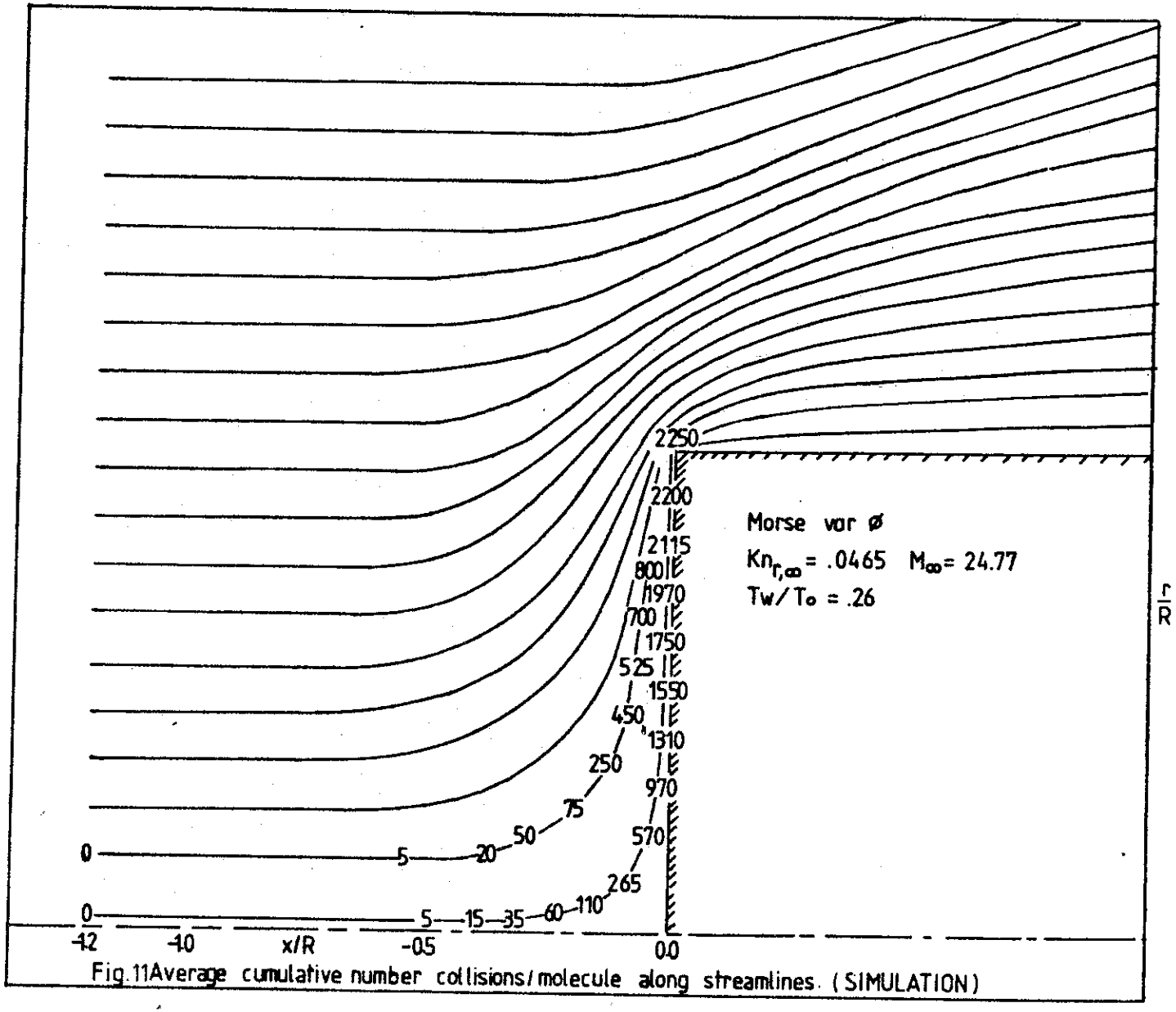

Fig.11Average cumulative number collisions/molecule along streamlines. (SIMULATION)

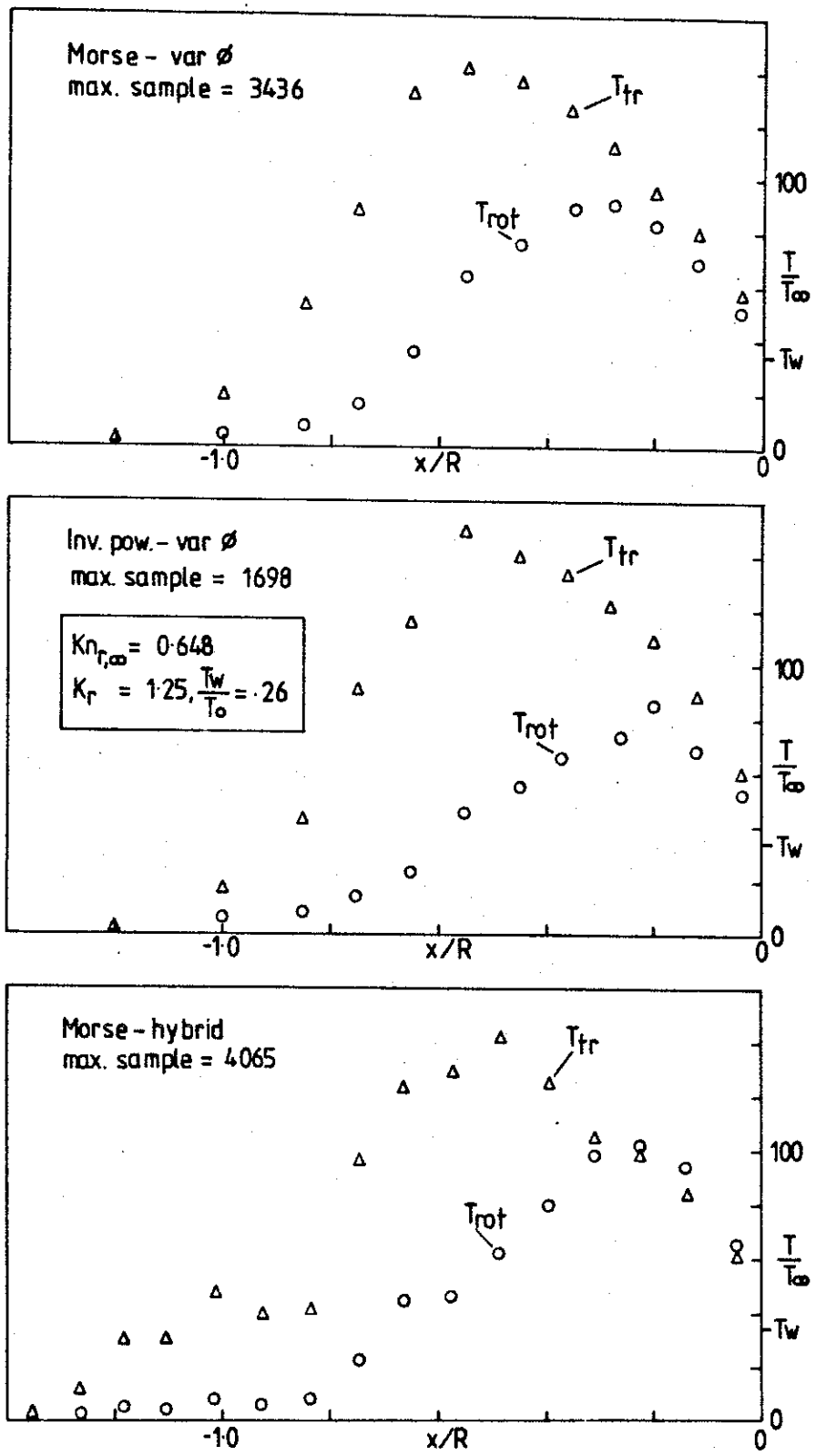

Fig. 12a STAGNATION LINE TEMPERATURE PROFILES

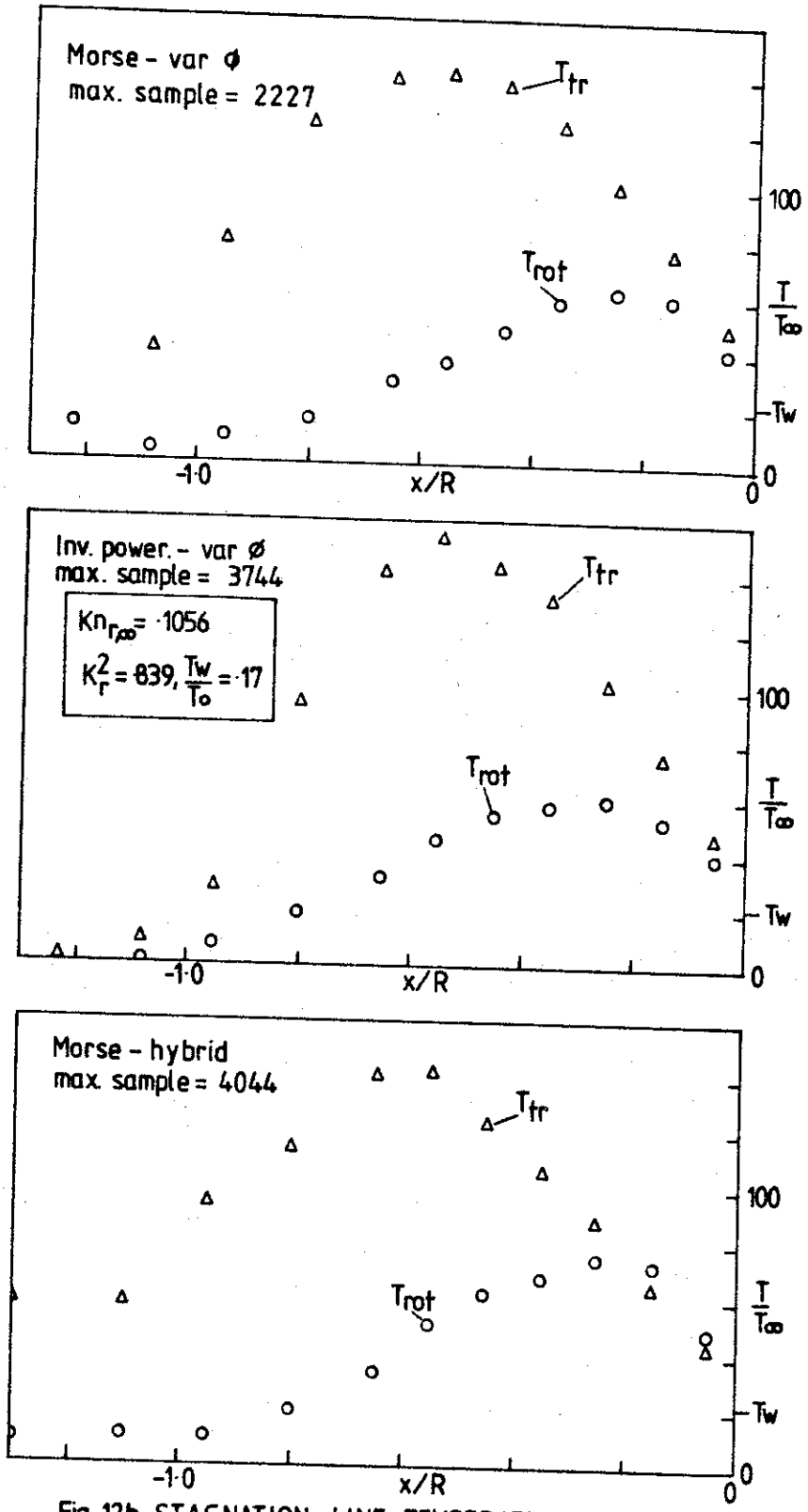

Fig. 12b STAGNATION LINE TEMPERATURE PROFILES

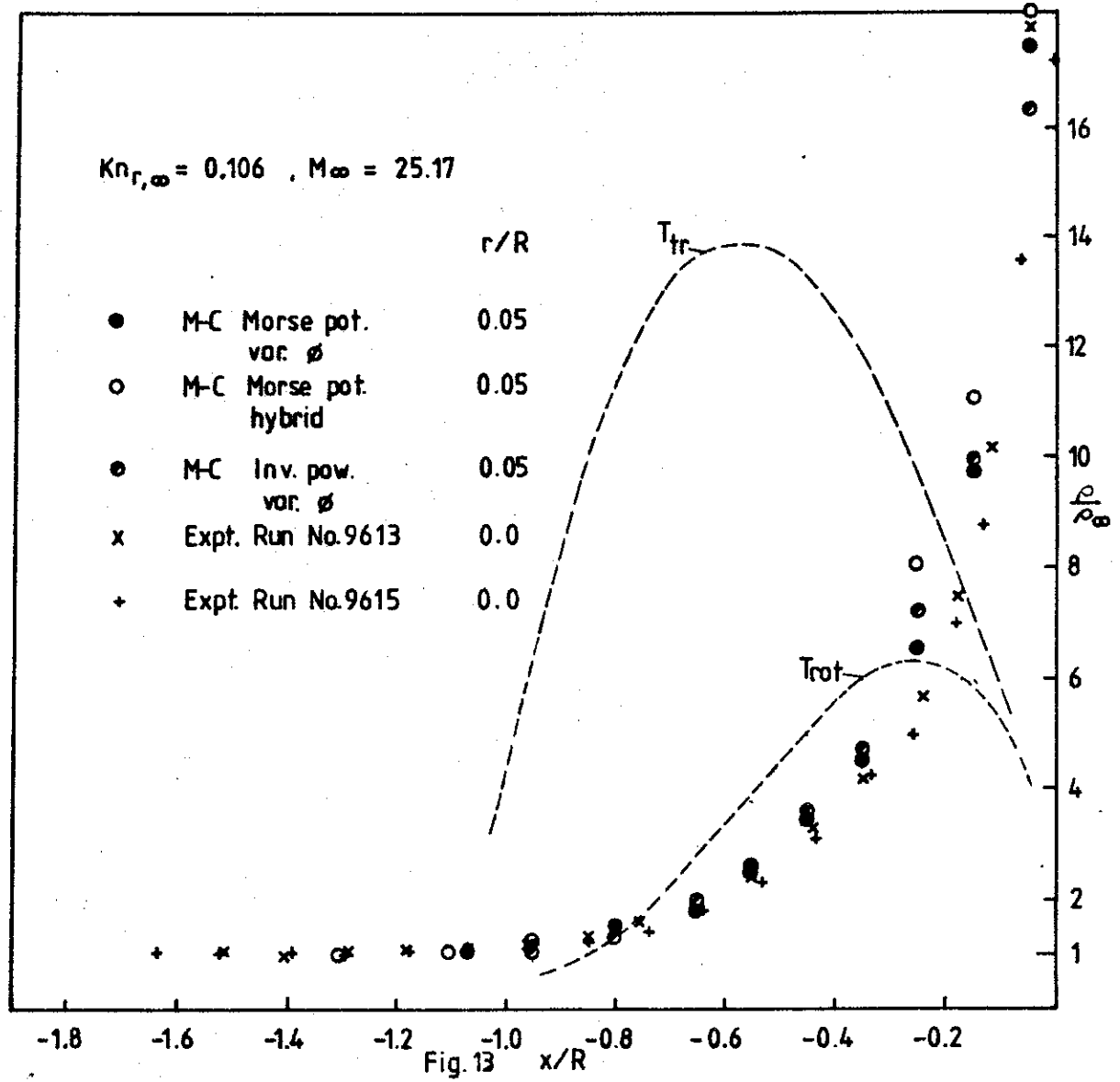
$Kn_{r,\infty}$ = 0.106 , M_∞ = 25.17
r/R
M-C Morse pot. var. ø 0.05
M-C Morse pot. hybrid 0.05
M-C Inv. pow. var. ø 0.05
Expt. Run No.9613 0.0
Expt. Run No.9615 0.0
T_{tr}
T_{rot}
ρ/ρ_∞
16
14
12
10
8
6
4
2
1
-1.8
-1.6
-1.4
-1.2
-1.0
-0.8
-0.6
-0.4
-0.2
x/R

Fig. 13

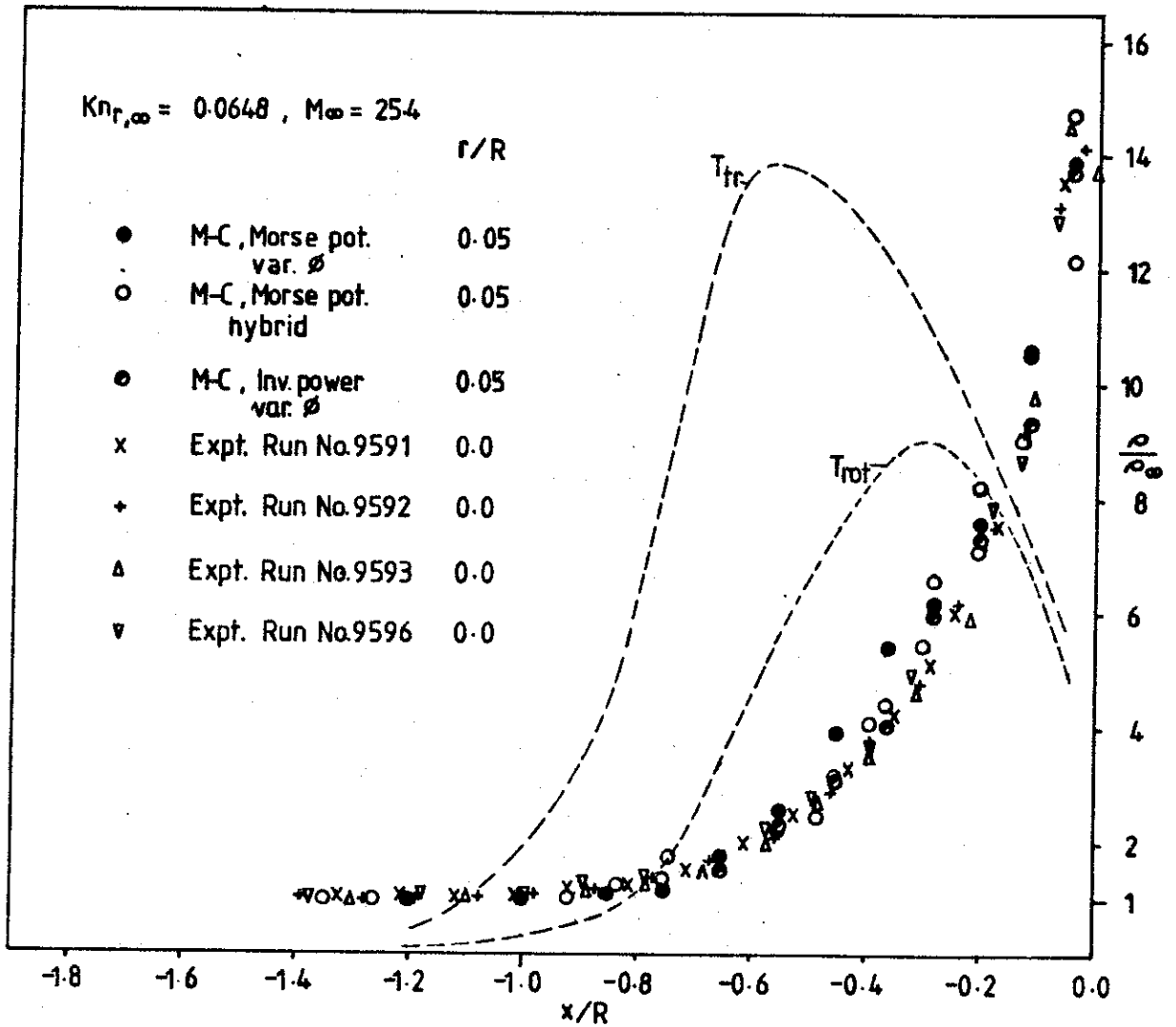
$Kn_{r,\infty}$ = 0.0648 , M_∞ = 25.4
r/R
M-C, Morse pot. var. ø 0.05
M-C, Morse pot. hybrid 0.05
M-C, Inv. power var. ø 0.05
Expt. Run No. 9591 0.0
Expt. Run No. 9592 0.0
Expt. Run No. 9593 0.0
Expt. Run No. 9596 0.0
T_{tr}
T_{rot}
$\frac{\rho}{\rho_\infty}$
x/R
16
14
12
10
8
6
4
2
1
-1.8
-1.6
-1.4
-1.2
-1.0
-0.8
-0.6
-0.4
-0.2
0.0

Fig. 14

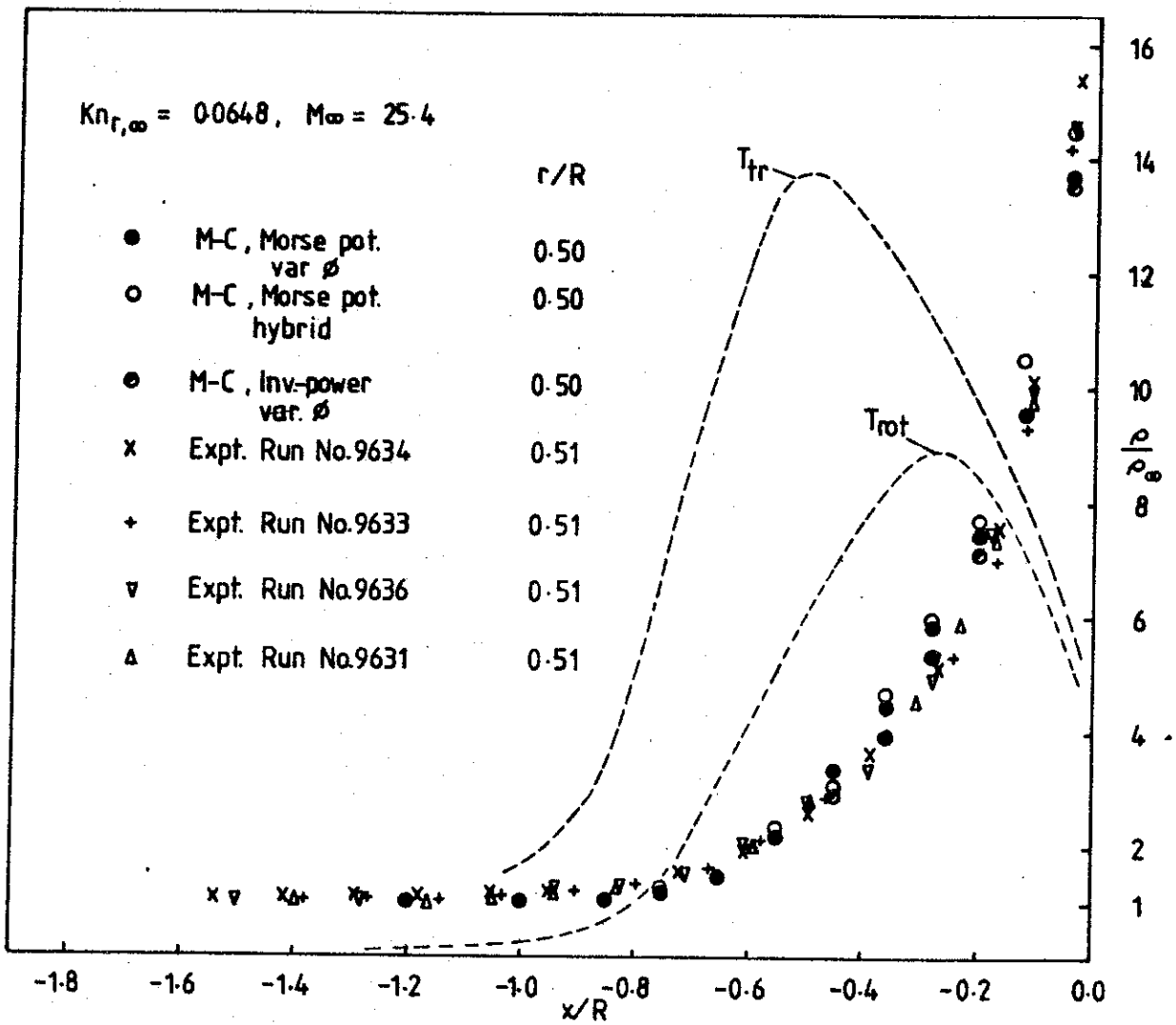
$Kn_{r,\infty}$ = 0·0648, M_∞ = 25·4
r/R
M-C, Morse pot. var ø 0·50
M-C, Morse pot. hybrid 0·50
M-C, Inv.-power var. ø 0·50
Expt. Run No.9634 0·51
Expt. Run No.9633 0·51
Expt. Run No.9636 0·51
Expt. Run No.9631 0·51
T_{tr}
T_{rot}
$\frac{\rho}{\rho_\infty}$
16
14
12
10
8
6
4
2
1
-1·8
-1·6
-1·4
-1·2
-1·0
-0·8
-0·6
-0·4
-0·2
0·0
x/R
Fig. 15

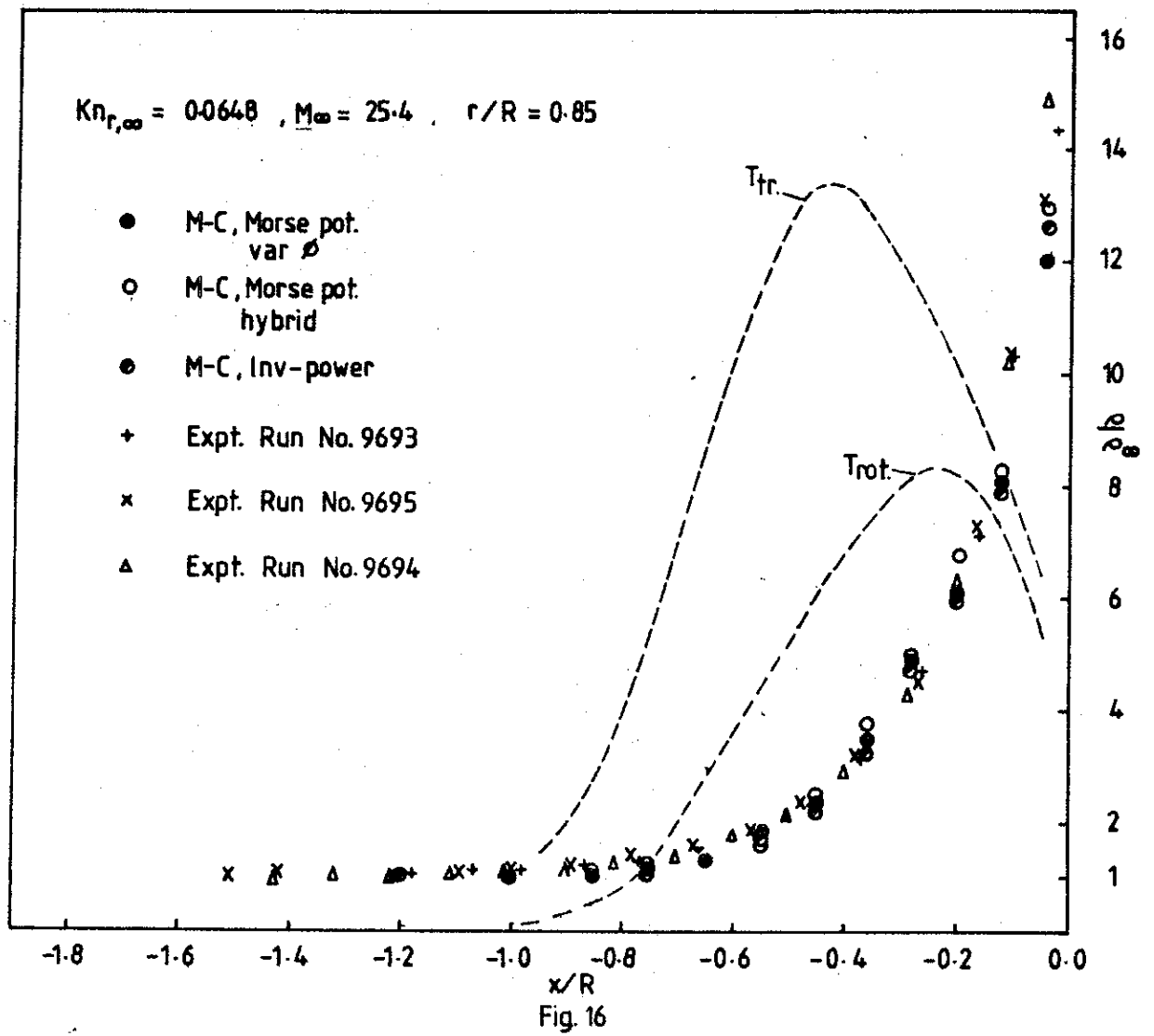
$Kn_{r,\infty}$ = 0·0648 , M_∞ = 25·4 , r/R = 0·85
M-C, Morse pot. var ∅
M-C, Morse pot. hybrid
M-C, Inv-power
Expt. Run No. 9693
Expt. Run No. 9695
Expt. Run No. 9694
$T_{tr.}$
$T_{rot.}$
16
14
12
10
8
6
4
2
1
ρ/ρ_∞
-1·8
-1·6
-1·4
-1·2
-1·0
-0·8
-0·6
-0·4
-0·2
0·0
x/R
Fig. 16

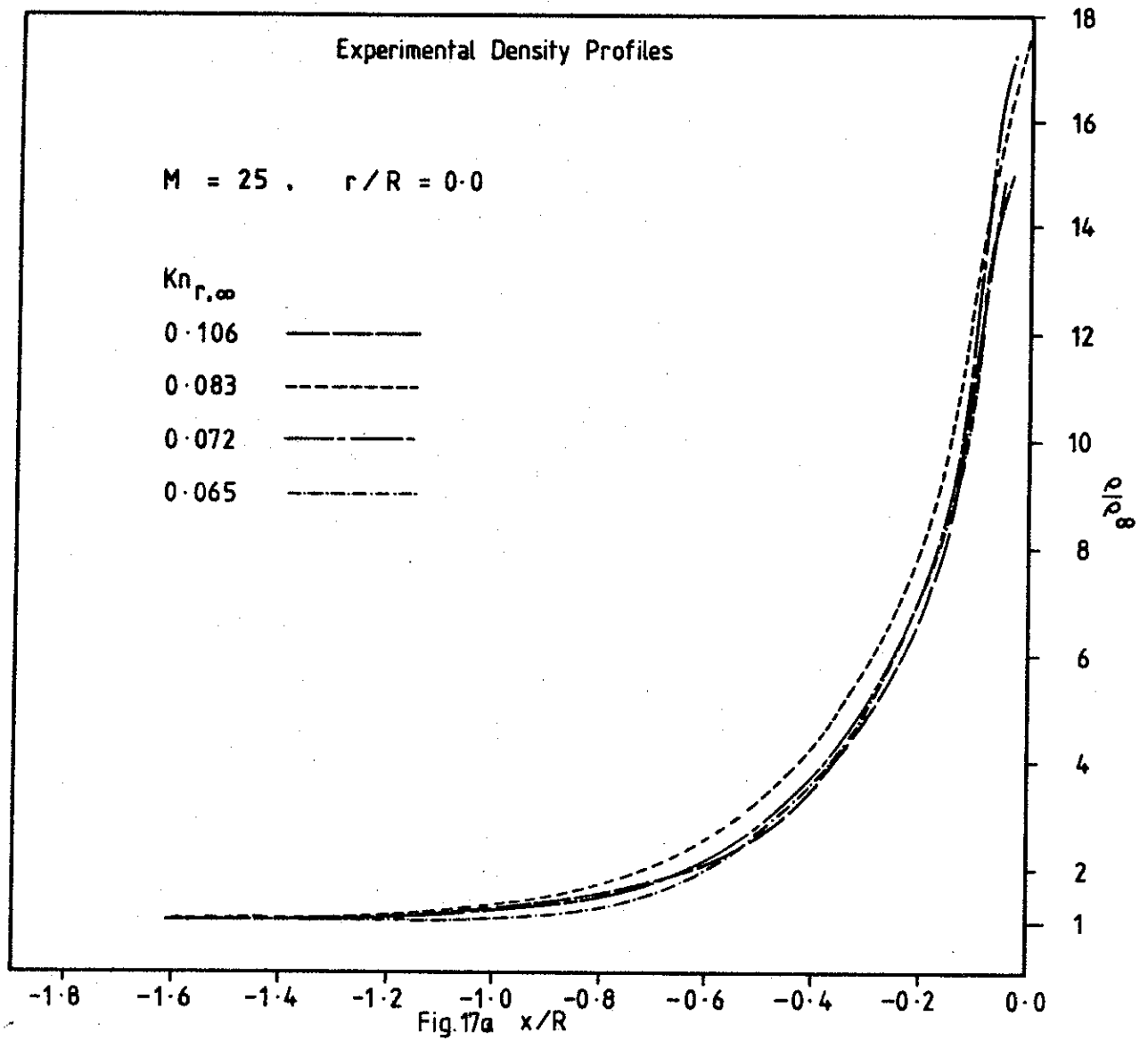
Experimental Density Profiles
M = 25 . r/R = 0·0
Kn r,∞
0·106
0·083
0·072
0·065
18
16
14
12
10
8
6
4
2
1
ρ/ρ∞
-1·8
-1·6
-1·4
-1·2
-1·0
-0·8
-0·6
-0·4
-0·2
0·0
x/R
Fig. 17a

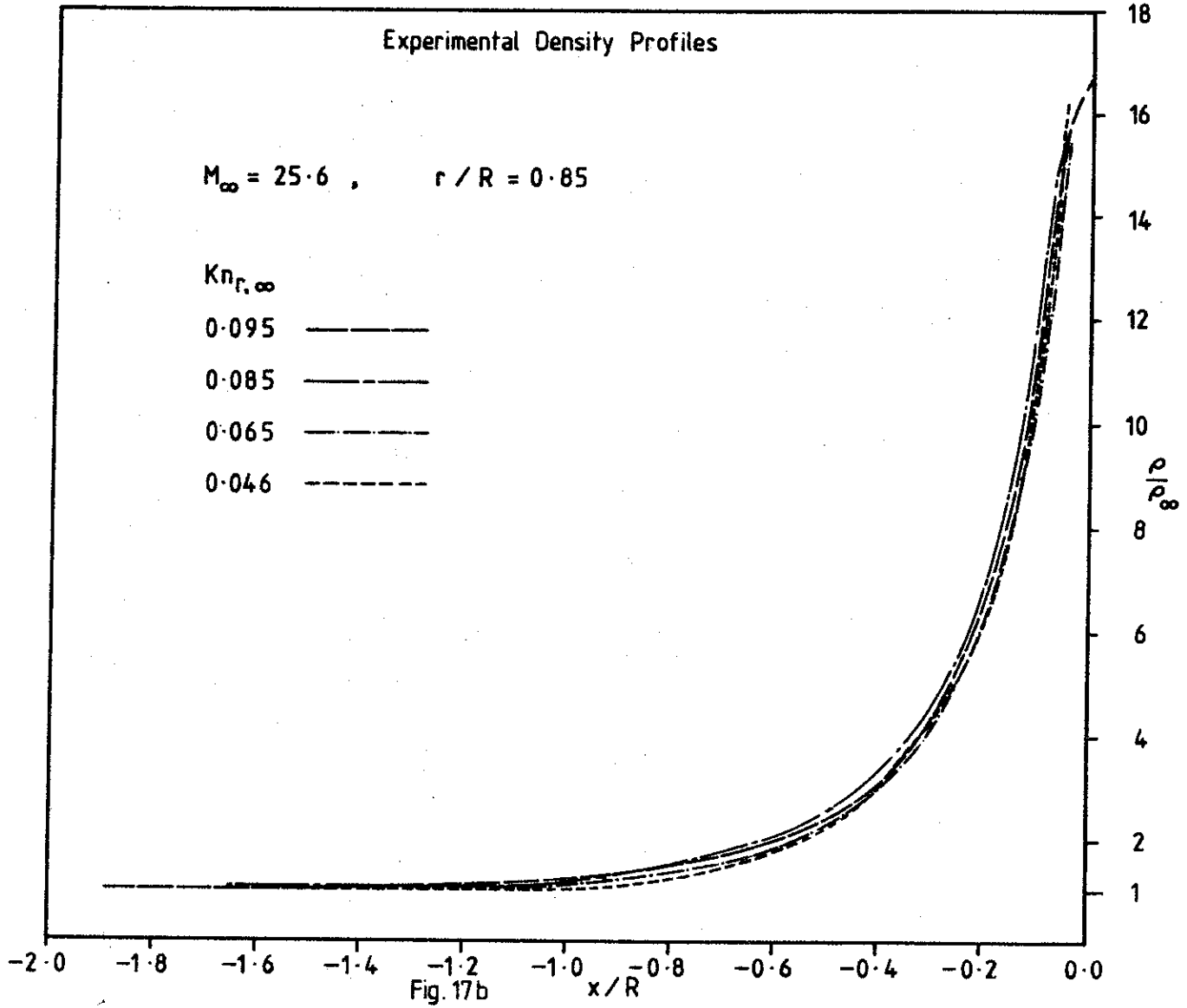
Experimental Density Profiles
$M_\infty = 25{\cdot}6$, $r / R = 0{\cdot}85$
$Kn_{r,\infty}$
0·095
0·085
0·065
0·046
18
16
14
12
10
8
6
4
2
1
$\frac{\rho}{\rho_\infty}$
−2·0
−1·8
−1·6
−1·4
−1·2
−1·0
−0·8
−0·6
−0·4
−0·2
0·0
x / R
Fig. 17b

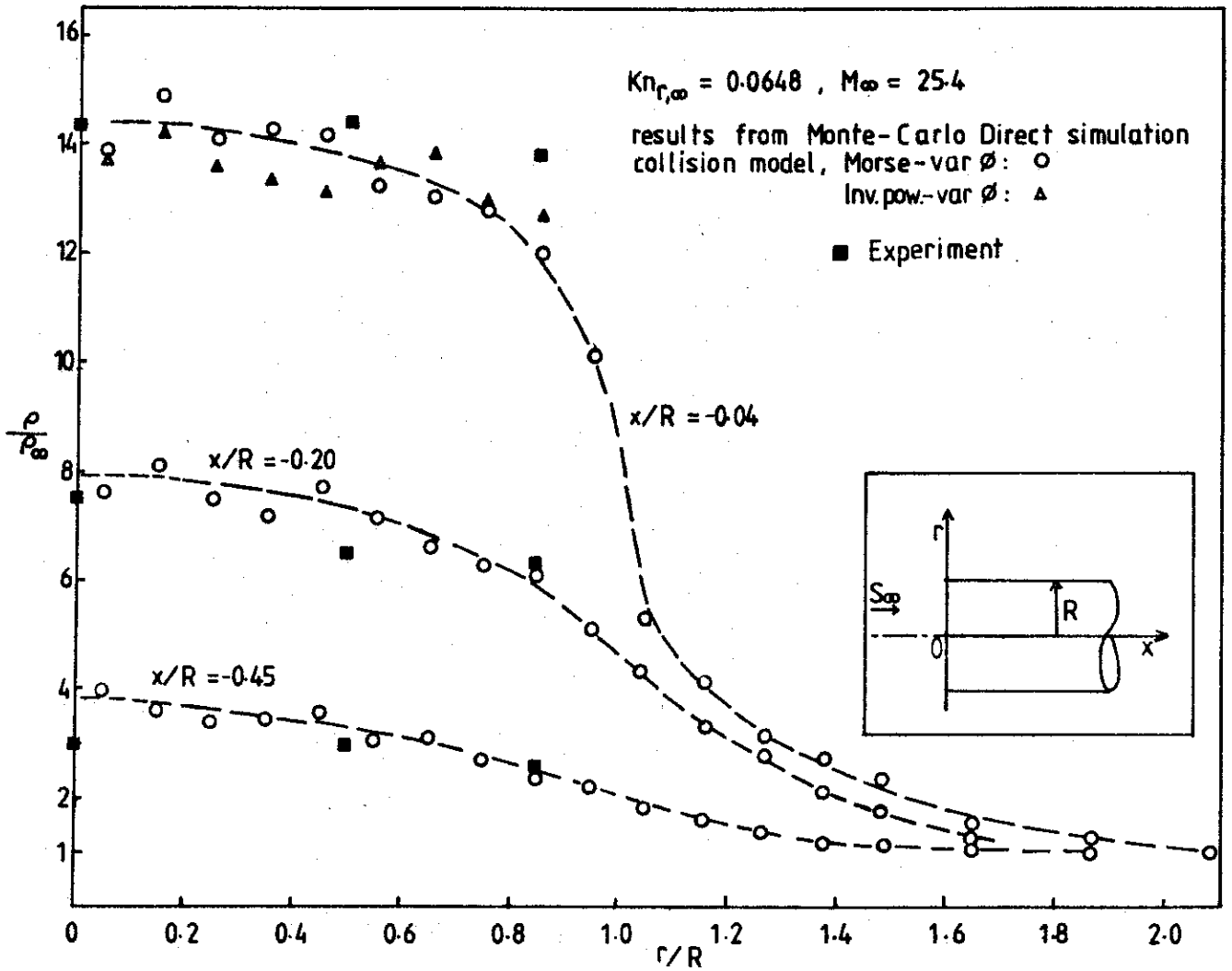

Fig. 18 Radial density distributions at various distances from cylinder face

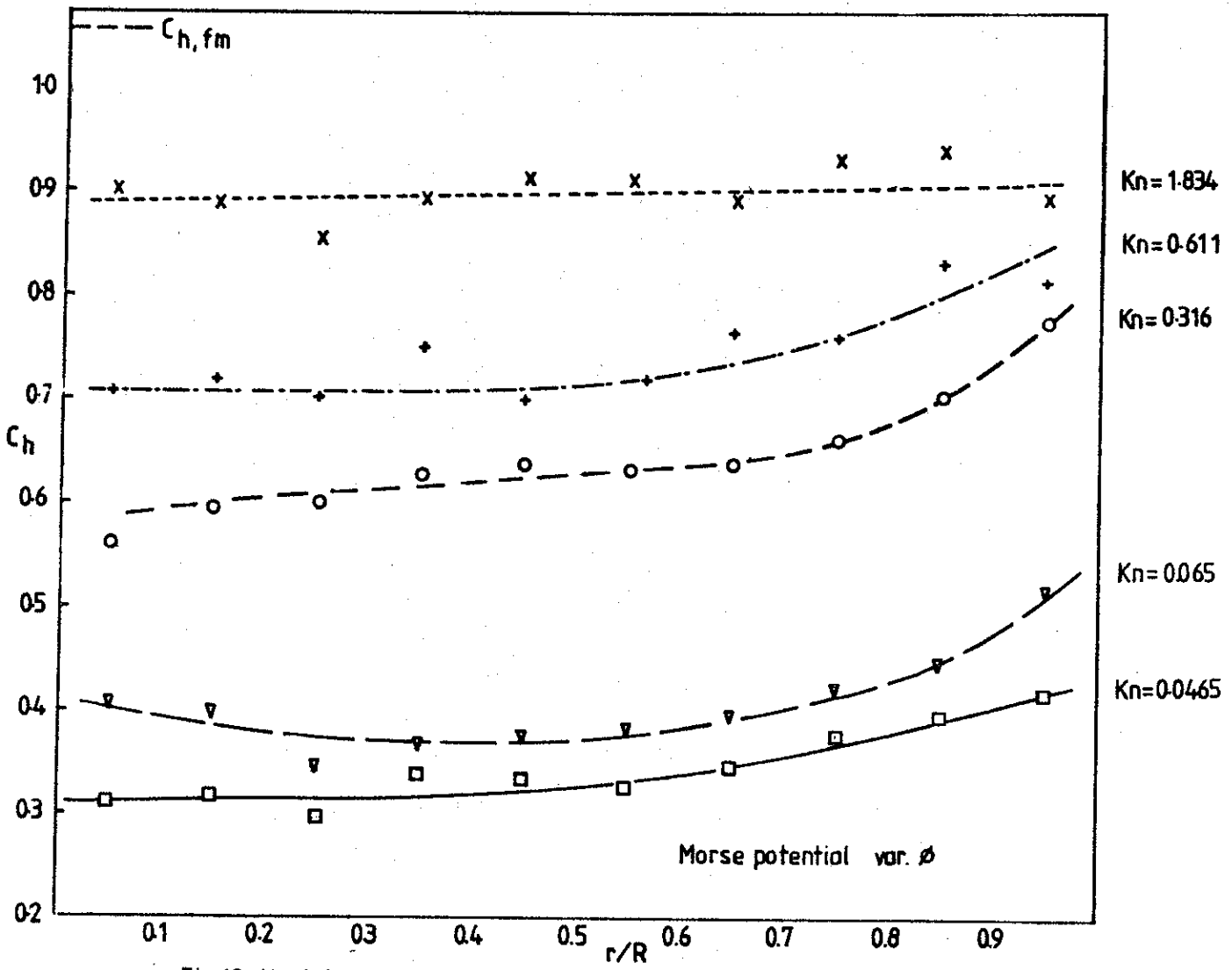

Fig.19 Heat transfer... distribution across cylinder face

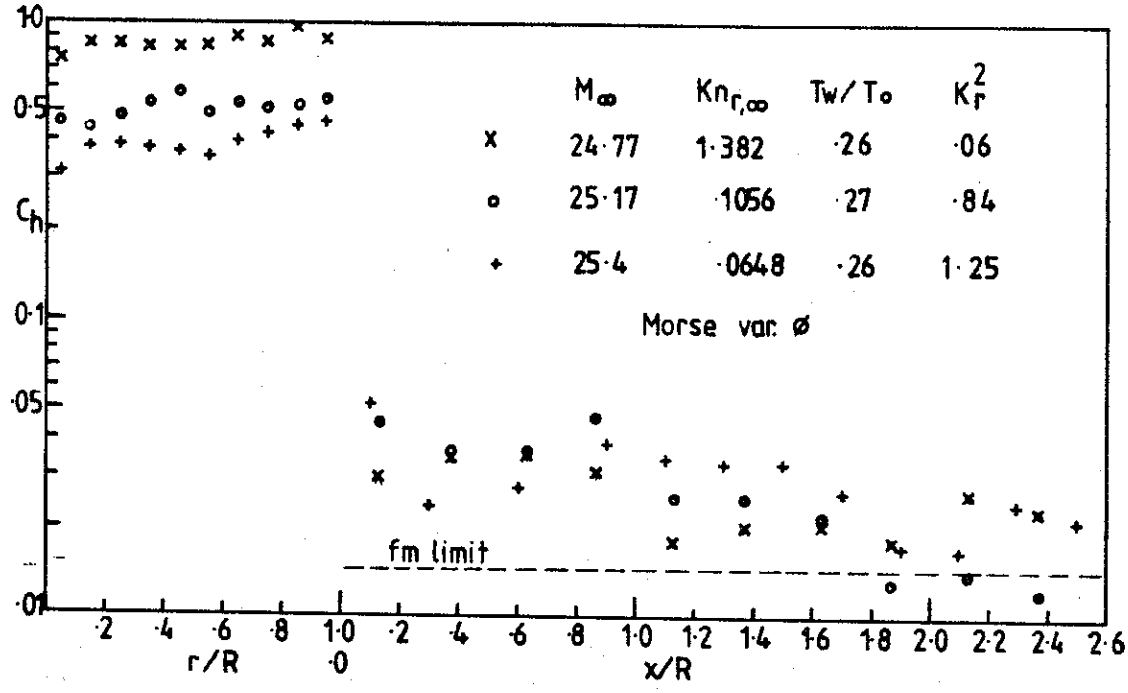

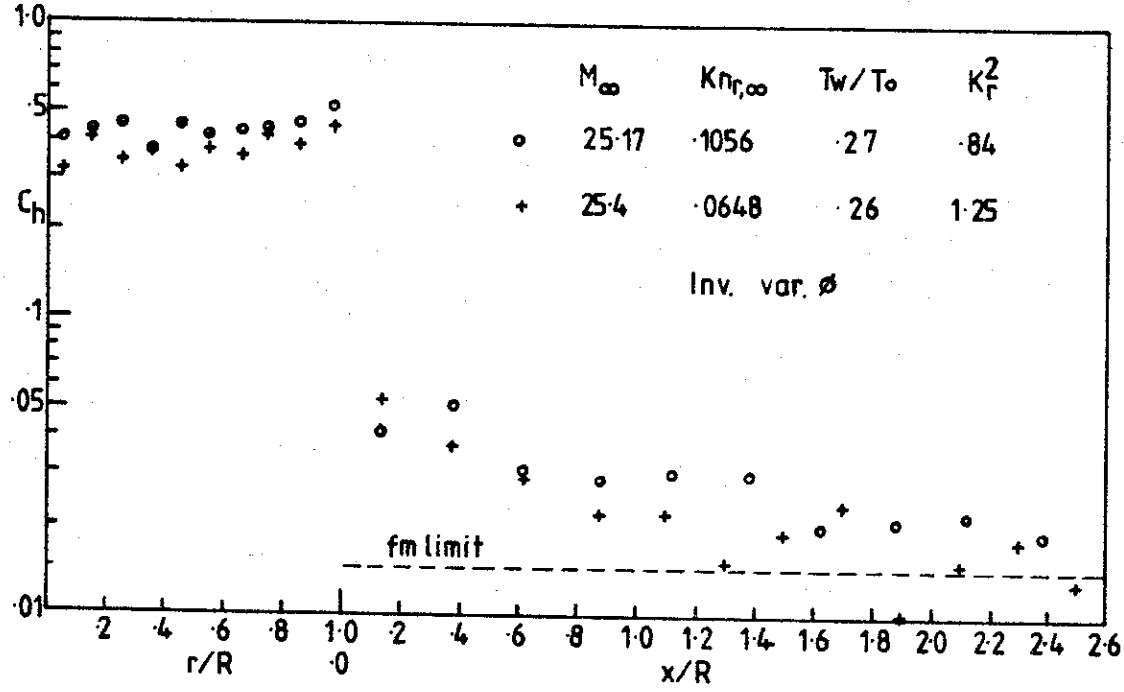

Fig. 20 Heat transfer - front face, side

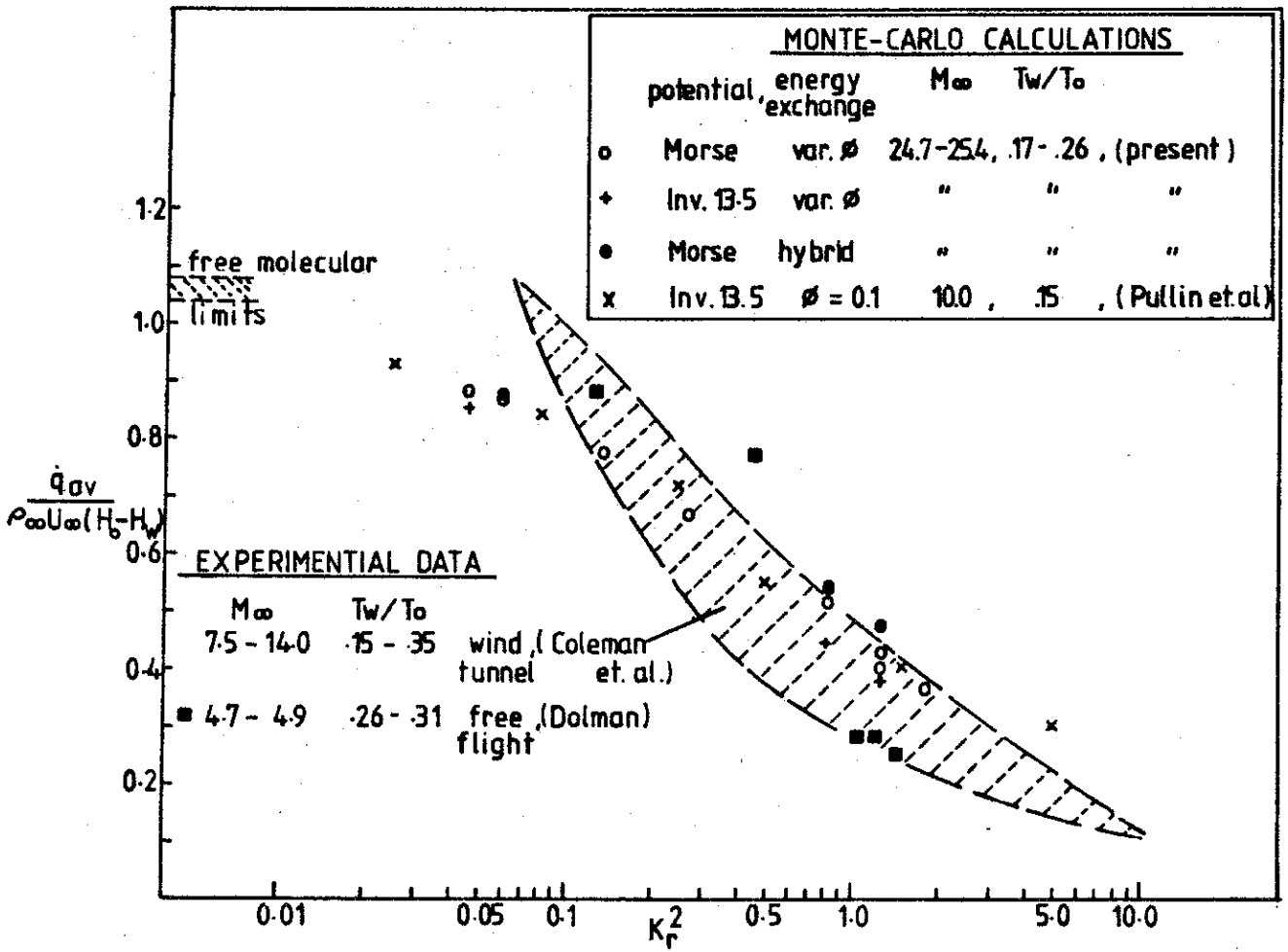

Fig. 21 Average heat transfer- front face bluff cylinders

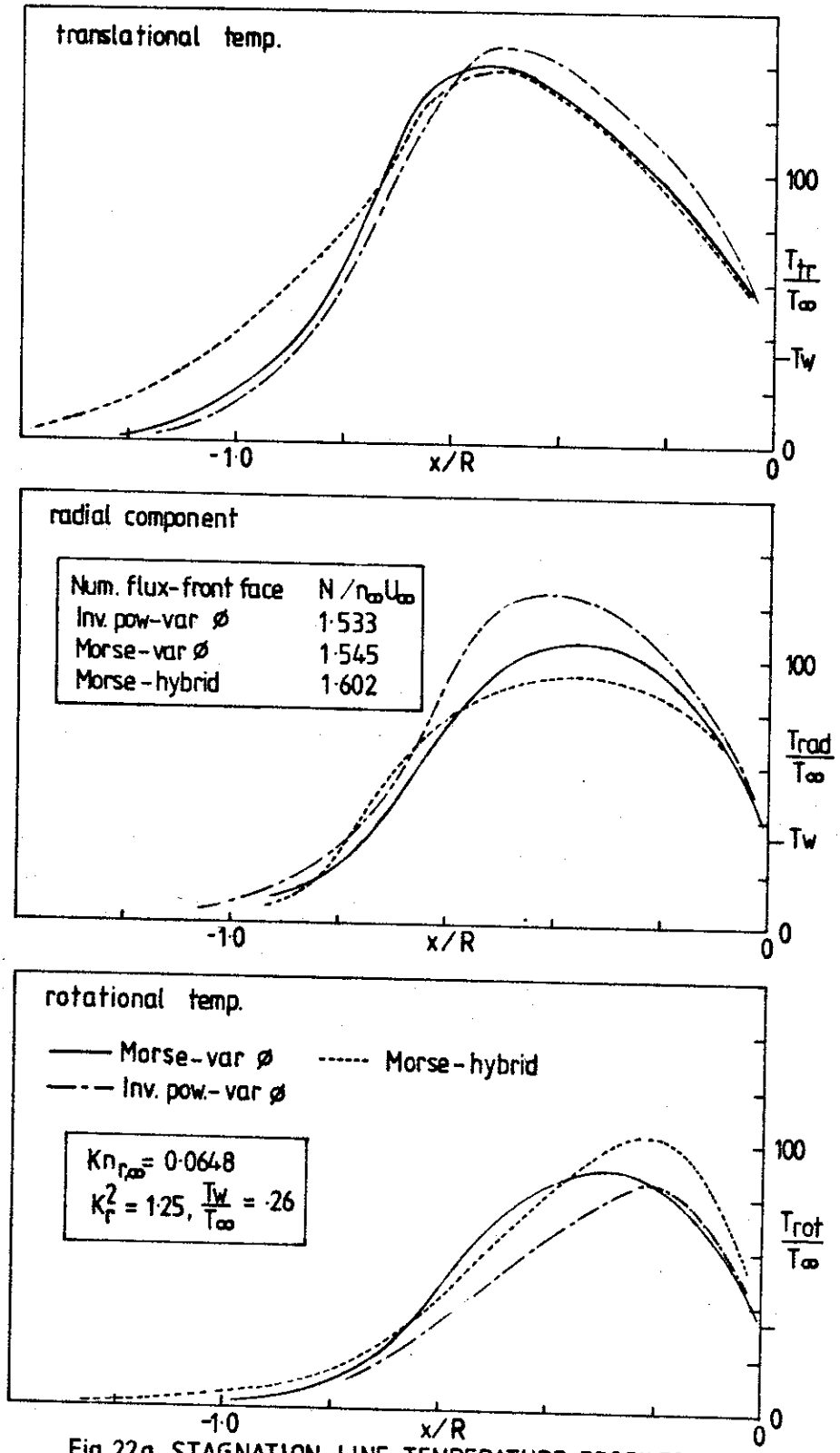

Fig. 22a STAGNATION LINE TEMPERATURE PROFILES

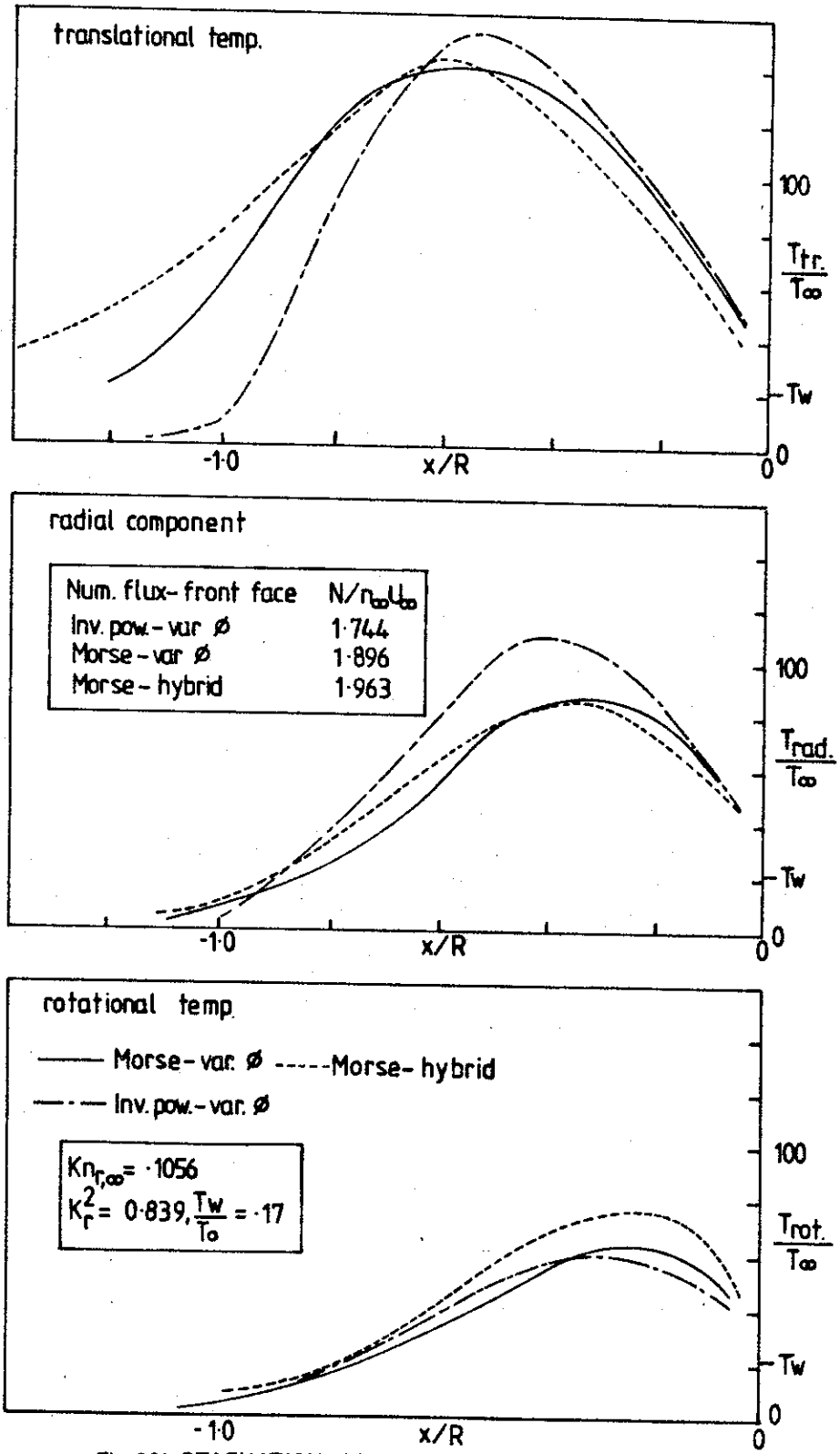

Fig 22b STAGNATION LINE TEMPERATURE PROFILES